Progress in Polymer Science 37 (2012) 1657–1677

Contents lists available at SciVerse ScienceDirect

Progress in Polymer Science

journal homepage: www.elsevier.com/locate/ppolysci

Poly(lactic acid) crystallization

Sajjad Saeidlou[a], Michel A. Huneault[a,*], Hongbo Li[b], Chul B. Park[c]

[a] Department of Chemical and Biotechnological Engineering, Faculty of Engineering, Université de Sherbrooke, Sherbrooke, QC J1K 2R1, Canada
[b] National Research Council of Canada, 75, de Mortagne, Boucherville, QC J4B 6Y4, Canada
[c] Department of Mechanical and Industrial Engineering, University of Toronto, 5 King's College Road, Toronto, ON M5S 3G8, Canada

ARTICLE INFO

Article history:
Received 25 April 2012
Received in revised form 13 July 2012
Accepted 16 July 2012
Available online 20 July 2012

Keywords:
Poly(lactic acid)
Polylactide
PLA
Crystallization
Kinetics
Review

ABSTRACT

Poly(lactic acid) is a biobased and compostable thermoplastic polyester that has rapidly evolved into a competitive commodity material over the last decade. One key bottleneck in extending the use of PLA is the control of its crystallinity. Understanding the crystallization behavior is particularly crucial to control PLA's degradation rate, thermal resistance as well as optical, mechanical and barrier properties. PLA crystallization has also been a particularly rich topic from a fundamental point of view because of the existence of the two enantiomeric forms of lactic acid that can be used to control the crystallization rate but also to form high melting point stereocomplex structures. This article presents an overview of the current understanding on the fundamentals of PLA crystallization in quiescent conditions and on the practical means to enhance its rate. Data from the abundant literature on PLA crystallization were compiled and analyzed to provide comprehensive relationships between crystallization kinetics and the main molecular structure characteristics of PLA. In addition, the most promising efforts in enhancing PLA crystallization kinetics through plasticization or heterogeneous nucleation were reviewed.

Contents

* Corresponding author. Tel.: +1 819 821 8000x65580; fax: +1 819 821 7955.
E-mail address: michel.huneault@usherbrooke.ca (M.A. Huneault).

0079-6700/$ – see front matter © 2012 Elsevier Ltd. All rights reserved.
http://dx.doi.org/10.1016/j.progpolymsci.2012.07.005

1. Introduction

Poly(lactic acid) or PLA is a biodegradable polymer that can be produced from annually renewable resources [1]. It is an aliphatic thermoplastic polyester that boasts a high modulus, high strength and good clarity. Therefore, it has raised a lot of interest as a potential replacement for petroleum-based polymers. Before its introduction as a packaging and commodity material, specialty grades of PLA had been developed for biomedical uses. Its biocompatibility and bioresorbability had made it a suitable choice for applications such as drug delivery systems, sutures, blood vessels, etc. The commercial introduction of bio-based PLA in 2003 has opened the way for more common applications. In particular, PLA has been finding an increasing number of applications in the packaging industry due to its good mechanical properties, transparency and compostability.

The term poly(lactic acid) is slightly misleading. The PLA now commercialized for commodity applications is made from ring-opening polymerization of lactide, a dimer of lactic acid. Therefore, from a nomenclature point of view, we should refer to polylactide rather than to poly(lactic acid) but both terms are used indifferently in the scientific literature. Another precision that needs to be made is that PLA does not refer to a single material but rather to a family of materials with a range of properties due to the chiral nature of lactic acid as we will explain later. One general drawback of the PLA family of material is that they exhibit a lower glass transition temperature (T_g), up to about 60 °C, compared to competing polyesters. The ubiquitous polyethylene terephthalate, for example, possesses a T_g around 80 °C. Therefore, unless PLA can be crystallized to a large extent, its thermal resistance will remain relatively poor. For example, heat deflection temperature (HDT) and Vicat penetration temperature were increased more than 30 and 100 °C respectively, after amorphous samples were fully crystallized. As well, an increase in flexural modulus and strength by 25% and increased impact resistance were reported following the full crystallization of amorphous PLA [2,3]. On the other hand, if one is interested in maintaining the PLA clarity or maximizing the biodegradability of PLA, it might be useful to understand how to limit crystallization. Enzymatic degradation rate can be reduced by more than 7 times for highly crystalline PLA compared to the amorphous samples [4]. Furthermore, barrier properties are improved due to PLA crystallization. A study by Drieskens et al. [5] showed for crystallized PLA that oxygen and water vapor permeability coefficients were decreased by more than 4 and 3 times respectively, compared to amorphous references. This stresses the importance of PLA crystallization not only from a fundamental point of view but also for obvious market development considerations. Several authors have reviewed the synthesis, properties, processing and applications of PLA [1,6–10]. The current review will focus specifically on the current understanding of PLA crystallization. In particular, we will examine the microstructure of PLA, the isothermal and non-isothermal crystallization kinetics and will summarize the different strategies used to control or enhance crystallinity development during melt processing operations.

2. Chain structure

To understand the crystallization behavior of PLA, it is useful to first examine its chain structure. PLA can be synthesized by two polymerization routes, polycondensation of lactic acid or ring-opening polymerization of lactide [8]. In both cases, lactic acid is the feedstock for PLA production. Due to an asymmetric carbon atom, lactic acid has two optically active forms called L-lactic acid and D-lactic acid. When producing PLA from lactide, three forms are possible: the LL-lactide made from two L-lactates, the DD-lactide from two D-lactates, and the LD or meso-lactide made from a combination of one L- and one D-lactate. In Fig. 1, schematics of the lactic acid and lactide molecules are illustrated.

The polymers coming from pure L- or pure D- feed are referred to as PLLA and PDLA respectively. Commercial PLA grades however are usually based on an L-rich mixture as the majority of bacteria used in fermentation processes produce L-lactic acid predominantly. Due to purification issues, they typically comprise a minimum of 1–2% *D* units. Since the two repeating units are optically active, they rotate polarized light in opposite directions. Specific optical rotation values in chloroform at 25 °C ($[\alpha]^{25}$) equal to −156° and +156° are commonly used in the literature for 100% pure PLLA and PDLA, respectively [11–15]. A higher content of one repeating unit in polymer chain results in a higher rotation angle in that direction. Thus, by employing the following equation [16], one can calculate the molar fraction of *D* units (X_D) in PLA:

$$X_D = \frac{[\alpha]^{25} + 156}{312} \quad (1)$$

Based on the molar fraction and source of *D* units in PLA chains, i.e., DD-lactide or meso-lactide, another important

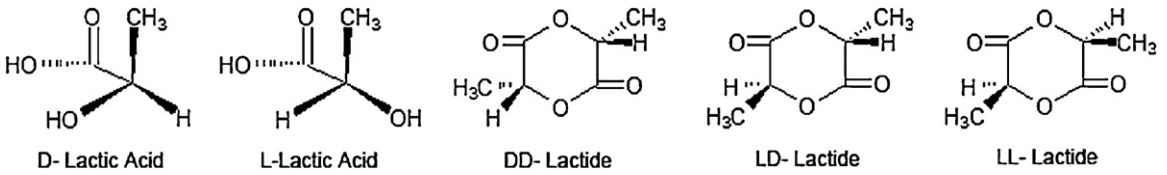

Fig. 1. Stereochemistry of lactic acid and lactide molecules.

parameter called the average isotactic sequence length ($\bar{\zeta}$) is defined for L-lactide rich PLA as:

$$\bar{\zeta} = \frac{a}{X_D} \tag{2}$$

where a is a coefficient that depends on the source of D units in polymerization feed. It is equal to 1 if all D units are incorporated via meso-lactide, equal to 2 if they are all comprised of DD-lactide and between 1 and 2 depending on the ratio of meso and DD-lactide in the polymerization feed. Using the coefficient 2 for DD-lactide is due to the paring of D units in the random copolymerization of LL-lactide and DD-lactide. Another clarification about the latter equation is that it is correct for random copolymers. In some cases by employing specific initiators it is possible to have a preferential monomer insertion into the growing chain resulting in a PLA with longer isotactic sequences compared to a statistical copolymer with the same X_D [13,14].

A higher $\bar{\zeta}$ value means a higher level of chain order. Therefore, this parameter influences directly the crystallization behavior of PLA. It can be controlled by adjusting the ratio of LL, DD and meso-lactide in the monomer feed for PLA polymerization. However, in the course of polymerization, L or D units may convert into their counterpart form [17]. This undesirable reaction called racemization will influence $\bar{\zeta}$ and thus will disturb chain order. Another way that chain order may be disturbed is by inter or intramolecular trans-esterification reactions [11].

Chain architecture is another aspect of chain structure. PLA is typically linear in its structure, but it is possible to produce it in different branched architectures by employing multifunctional initiators [18–20] or co-monomers bearing initiation groups [21,22] in polymerization reaction. Multifunctional chain extenders [23,24] or peroxides [25,26] sometimes used for PLA to counterbalance chain scission are other potential sources of branching. Accordingly, it is useful to understand the effect of branching parameters such as branch's length, amount and architecture on PLA crystallization behavior.

3. Crystal structure

Different crystal structures have been reported for PLA, the formation of which depends on the crystallization conditions. The most common α-form occurring in conventional melt and solution crystallization conditions was first reported by De Santis and Kovacs [27] and investigated further in a number of studies [28–30]. Based on WAXD and IR data, Zhang et al. reported the slightly different α′-form for PLA crystallized below 120 °C [31]. The chain conformation and crystal system of the α′-form is similar to α structure, but with a looser and less ordered chain packing. More recent studies suggest that only the α′ crystal is formed at crystallization temperatures below 100 °C while crystallization between 100 and 120 °C gives rise to the coexistence of α′ and α crystal structures [32,33]. As a consequence of its looser chain packing and disordered structure, the α′ crystal leads to a lower modulus and barrier properties and to higher elongation at break compared to α crystal [34]. A β-form, first observed by Eling et al. [35], is created by stretching the α-form at high draw-ratio and high temperature such as in hot-drawing of melt or solution spun fibers [29,35]. Melting temperature of the β structure is about 10 °C lower compared to the α crystal, implying that β form is thermally less stable [29]. Later, Puiggali et al. [36] suggested that β-form crystal is a frustrated structure with a trigonal cell containing three chains which are randomly oriented up and down. A more ordered crystal modification called γ was also reported by the same group [37]. In the γ-form which was obtained by epitaxial crystallization of PLA on hexamethylbenzene, two chains are oriented antiparallel in the crystal cell. Besides the homo-crystallization of PLLA and PDLA, these two enantiomeric chains can co-crystallize together and form a stereocomplex [38]. In contrast to PLLA or PDLA homocrystals, the stereocomplex crystal cell contains one PLLA and one PDLA chain. Interestingly, melting point of the stereocomplex is about 50 °C higher than that of PLA homocrystal. Thus, stereocomplexation may provide greater temperature resistance to the material. Properties of PLA crystal form are summarized in Table 1. The densities were calculated based on the reported cell parameters and the number of monomers in each unit cell.

4. Structure–properties relationship

4.1. Glass transition temperature

The glass transition temperature, T_g, plays an important role on the determination of PLA crystallization window since polymer chain mobility is related to $T - T_g$. Fig. 2 presents T_g data as a function of molecular weight for different D-lactate contents. The T_g increases rapidly when the molecular weight is increased to 80–100 kg/mol but then reaches a constant value. At a given molecular weight, an increase in optical impurity, i.e. increase in minor unit concentration (defined as D-lactate in the case of an L-rich PLA and as L-lactate for a D-rich PLA), decreases the glass transition temperature to some extent but its effect on T_g is not as significant as on T_m.

Table 1
Properties of different PLA crystal types.

Crystal type	Crystal system	Chain conformation	Cell parameters						$\rho_{theoretical}$ (g/cm^3)
			a (nm)	b (nm)	c (nm)	α (°)	β (°)	γ (°)	
α [27]	Pseudo-orthorombic	10_3 helical	1.07	0.645	2.78	90	90	90	1.247
α [30]	Orthorombic	10_3 helical	1.05	0.61	2.88	90	90	90	1.297
β [29]	Orthorombic	3_1 helical	1.031	1.821	0.90	90	90	90	1.275
β [36]	Trigonal	3_1 helical	1.052	1.052	0.88	90	90	120	1.277
γ [37]	Orthorombic	3_1 helical	0.995	0.625	0.88	90	90	90	1.312
SC [39]	Triclinic	3_1 helical	0.916	0.916	0.870	109.2	109.2	109.8	1.274
SC [40]	Trigonal	3_1 helical	1.498	1.498	0.87	90	90	120	1.274

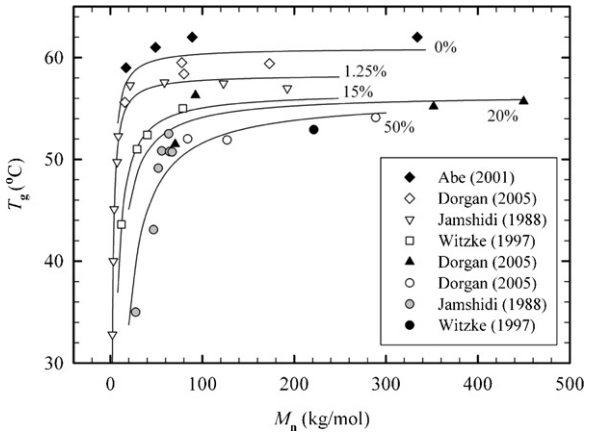

Fig. 2. T_g vs. M_n for different D-lactate concentrations. Data adapted from [41–44].

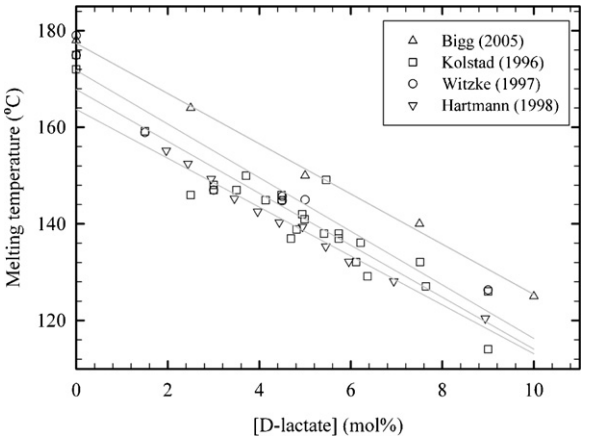

Fig. 3. Melting temperature as a function of D-lactate content. Data adapted from [44,47–49].

The data points for different D-lactate contents presented in Fig. 2 have been fitted with the predictions of the Flory–Fox equation given by

$$T_g = T_g^{\infty} - \frac{K}{M_n} \tag{3}$$

where T_g^{∞} is the glass transition temperature for infinite molecular weight, K is a constant and M_n is the number-average molecular weight. Accordingly, we have found that K increases linearly with D-lactate concentration and that T_g^{∞} shows a decreasing trend that can be predicted quite well with a rational function.

$$T_g^{\infty} = \frac{13.36 + 1371.68X_D}{0.22 + 24.3X_D + 0.42X_D^2} \tag{4}$$

$$K = 52.23 + 791X_D \tag{5}$$

where T_g^{∞} and K are respectively expressed in °C and in °C kg/mol.

The solid curves in Fig. 2 are the relationships obtained using Eq. (3) and the equation parameters T_g^{∞} and K described above, showing that T_g of PLA can be correctly estimated from these equations.

PLA chain architecture is another influential parameter for T_g. Compared to the linear structure, a branched PLA has a lower T_g value. This is due to the existence of a higher free volume caused by the higher number of chain ends. Pitet et al. [21] reported a 10 °C decrease in T_g for hyper branched PLA produced by copolymerization of lactide and glycidol while Zhao et al. [45] reported a 5 °C decrease in T_g for a 32-arms star shaped PLA produced by a poly(amido amine) dendrimer initiator. For lower branching contents such as star or comb like architectures with 4–9 arms [20] or by adding chain extender [46], no significant difference in T_g was reported.

4.2. Melting temperature and equilibrium melting point

Fig. 3 compares the melting point data from several authors as a function of *D*-unit content in the polymer structure. Pure PLLA (0% data) exhibits the maximum melting temperature, between 175 and 180 °C depending on authors. The melting point decreases linearly with the D-lactate content. The best linear fit for each data set is presented as well. The slope of these lines varies between −5.5 and −5.0, meaning that 1% *D*-unit content results in approximately 5 °C reduction in melting temperature. The difference between data presented in Fig. 3 is due to the different molecular weight. For example, Kolstad reported T_m for PLA with M_n between 50 and 130 kg/mol [47] while data reported by Witzke [44] and Bigg [48] concern PLA with M_w higher than 100 kg/mol. Furthermore, the thermal history applied by the authors differed slightly.

The melting temperature of a polymer is expected to increase with the temperature at which it was crystallized (T_c). Due to the kinetic barrier for crystallization when approaching the melting temperature, polymer crystallization is typically carried out at high undercoolings which limits the crystal thickness. However, in the limiting

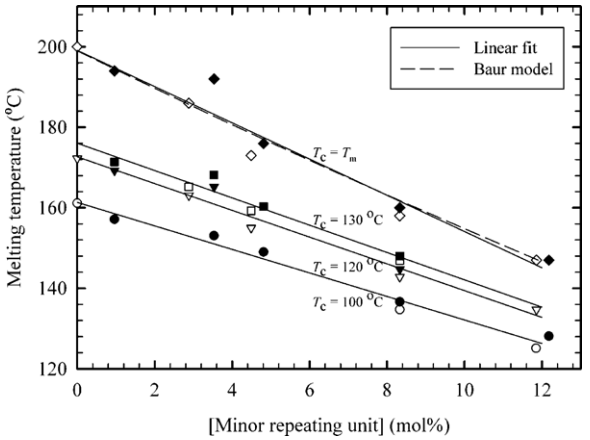

Fig. 4. T_m and T_m^0 as a function of minor repeating unit concentration, filled symbols for PDLA and open symbols for PLLA.
Data adapted from [16].

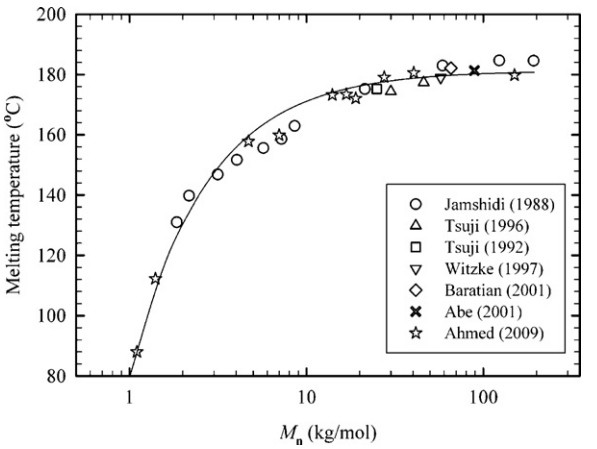

Fig. 5. PLA Melting point as a function of molecular weight.
Data adapted from [16,41,43,44,54,63,64].

case when crystallization is in equilibrium with melting of crystals, the crystal grows large enough in all directions so that the melting point reaches its maximum value, the so-called equilibrium melting point (T_m^0). The effect of the *D*-content on the T_m^0 of PLA can be calculated based on Hoffman–Weeks procedure [50]. Fig. 4 addresses the effect of crystallization temperature and of minor unit concentration on melting point and presents the T_m^0 values obtained for each minor unit concentration (i.e. the $T_c = T_m$ line). As expected, T_m decreases with minor unit concentration for all crystallization temperature. The melting point for any given minor unit content clearly increases as a function of the crystallization temperature. The data at $T_c = T_m$ is compared to the Baur Model prediction. This model is used to calculate melting point depression due to random copolymerization with a non-crystallizable co-monomer. The Baur model [51] is a modification based on earlier development proposed by Flory [52] and is given by

$$\frac{1}{T_m^0(\text{copolymer})} - \frac{1}{T_m^0(\text{homopolymer})} = -R\frac{(\ln X - (1/\bar{\zeta}))}{\Delta H_m^0} \quad (6)$$

where *X* is the molar fraction of crystallizable units, ΔH_m^0 is the equilibrium enthalpy of fusion, *R* is the gas constant and $\bar{\zeta}$ is the average sequence length of crystallizable units (see Eq. (2)). The model is identical to the one proposed by Flory except for the $1/\bar{\zeta}$ term. The equilibrium melting point depression is well described by the Baur Model. The validity of the Baur equation was also reported by Huang et al. [53] as well as Baratian et al. [54] for PLA systems.

The reported equilibrium melting temperature and equilibrium enthalpy of fusion of PLA are summarized in Table 2 with their calculation methods. Most authors report equilibrium melting temperatures between 200 and 215 °C. Variations may be due to variations in molecular weights and purity of the investigated polymers. In terms of equilibrium melting enthalpies, estimations vary between 80 and 135 J/g.

Molecular weight is another factor that significantly influences the melting temperature. Fig. 5 illustrates the melting point variation with the number averaged molecular weight M_n. The data has been compiled from seven papers where the PLA had less than 1.25% minor units [16,41,43,44,54,63,64]. The melting temperature increases dramatically with molecular weight for low M_n but reaches an asymptotical value at $M_n > 100$ kg/mol. It can be as low as 90 °C for PLA oligomers and increases up to 185 °C for PLA in the 100 kg/mol range. It is noteworthy that commercial PLA grades with a molecular weight in the 50–150 kg/mol range are in the high-molecular weight plateau region and therefore are not highly sensitive to molecular weight changes. In order to express the relationship between melting point and molecular weight in a simple way, the data from Fig. 5 was fitted using the following equation:

$$T_m = T_m^\infty - \frac{A}{M_n} \quad (7)$$

with $T_m^\infty = 181.3$ °C and $A = 1.02 \times 10^5$ °C g/mol. This is a common molecular weight dependency used for expressing changes in polymer properties such glass transition temperature, tensile strength, etc. The property is expressed as a function of the number-averaged molecular weight M_n, and of a theoretical property value obtained at infinite molecular weight. As can be seen on the figure, Eq. (7) gives a fair account of the effect of molecular weight on the melting temperature.

In some circumstances, two peculiarities are observed in the DSC heating scans of semi-crystalline PLA. One is the emergence of a small exothermic peak just before the melting peak and the other one is the occurrence of a double melting peak. These two phenomena can be well explained by taking into consideration the crystallization conditions in parallel with the α′ and α crystal formation requirements [32,33,65,66]. When PLA is crystallized at temperatures corresponding to α′ crystal formation, the small exotherm appearing just before the single melting peak is due to the transformation of disordered α′ crystals

Table 2
Reported equilibrium melting temperature and melting enthalpy for PLA.

T_m^0 (°C)			ΔH_m^0 (J/g)		
Method	Value	Ref.	Method	Value	Ref.
Hoffman-Weeks	200	[16]	Baur	82	[16]
Baur	199				
Gibbs–Thomson	214	[53]	–	100	[53]
Data fitting	215				
Hoffman-Weeks	207	[55]	Extrapolation to infinite crystal thickness	81 93	[56]
Hoffman-Weeks	205	[57]			
Hoffman-Weeks	206	[58]	Flory model for solution grown crystals		
Hoffman-Weeks	211, 212	[59]			
Hoffman-Weeks	215	[60]			
Hoffman-Weeks	215 ± 10	[28]	Extrapolation to crystal density (density-enthalpy relation)	135	[61]
Marand	227	[41]			
Hoffman-Weeks	199				
Hoffman-Weeks (pseudo-equilibrium lamellar crystals)	215	[62]			

to the ordered α-form. On the other hand, a double melting behavior appears when the crystallization temperature is situated in the region of simultaneous α′ and α type formation. For high crystallization temperatures, only α crystals are produced leading to a single melting peak.

Effect of branched structure on the melting point was also reported in a number of studies [20,23,45,46,67]. T_m was insensitive to branching when different contents of reactive copolymers (chain extenders) were employed to produce long chain branched PLA [23,46]. However, in the case of star-shaped PLAs synthesized by multifunctional initiators, the magnitude of T_m reduction was in direct relation with the number of arms. T_m reduction between 5 and 40 °C were observed for branched PLAs with 4–9 arms [20,67] and 32 arms [45], respectively. This behavior was attributed to the poor folding property of branched architecture due to steric hindrance as well as crystal imperfections caused by chain ends and branching points.

4.3. Maximum achievable crystallinity

Both the molecular weight and D-Lactate content determine the maximum achievable crystallinity. The enthalpy of fusion data obtained from various data sets are summarized in Fig. 6. The maximum enthalpy of fusion decreases generally with molecular weight and minor unit concentration. The molecular weight effect can be explained by the higher restrictions of chain motion at higher molecular weights, while the reduction in maximum achievable crystallinity by increasing D-lactate content is expected from crystal disruption. At about 10–12 mol.% (in the case of random distribution) of non-crystallizable unit, crystallinity is extremely low and so lengthy that PLA can be considered completely amorphous. Furthermore, crystallinity is diminished if branching is imparted to PLA structure as a consequence of more difficult chain segment transportation to crystallization sites. Compared to linear PLA, 7–15% less crystallinity was achieved for star-shaped and long chain branched PLA [20,23,45,67].

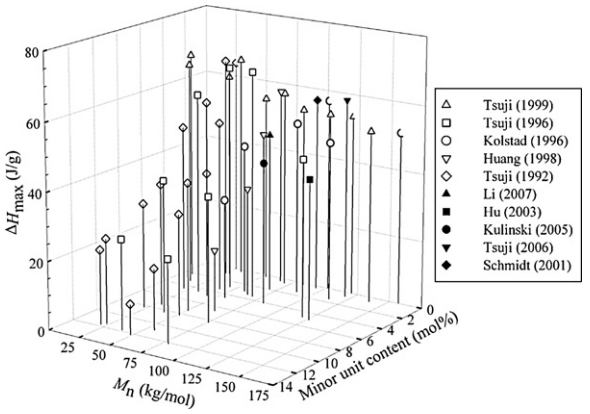

Fig. 6. Effect of molecular weight and minor unit concentration on maximum enthalpy of fusion.
Data adapted from [16,47,53,63,68–73].

5. Crystallization kinetics

5.1. Kinetics through visual observation

The overall crystallization kinetics is typically examined in terms of two independent phenomena: initial crystal nucleation and of subsequent crystal growth. In practice, optical microscopy on thin polymer films is used to determine the nucleation density and spherulite growth rates in isothermal conditions. The polymer film is usually first melted and rapidly cooled to the desired temperature. The size and number of spherulites can then be monitored over time. High-quality images and more accurate measurements are also reported by observation via an atomic force microscopy technique [74,75]. The relation between the number of crystallization sites (spherulite density) with crystallization temperature for PLA is illustrated in Fig. 7. The spherulite density was shown to decrease with temperature and the decreasing rate gradually accelerates with temperature.

The growth phenomenon is evaluated by measuring spherulite radius with time. The crystal growth rate (G)

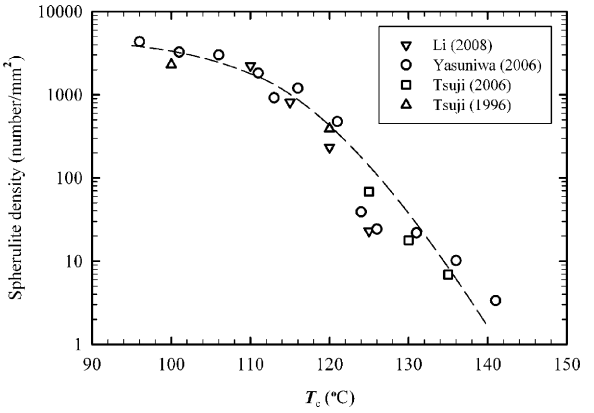

Fig. 7. Spherulite density as a function of crystallization temperature, Data adapted from [16,72,76,77].

is equal to the slope of the spherulite radius vs. time curve, while extrapolation of this data to zero-radius can be used to determine the induction time (related to nucleation kinetics). Usually G is constant for a specific T_c, implying a constant concentration of impurities like non-crystallizable segments at the growth front because of their rejection to inter-lamellar regions. One of the most important theories on polymer crystallization is the Hoffman–Lauritzen theory that deals with the crystal growth kinetics [78,79]. It defines three crystallization regimes based on the ratio between the rate of surface nucleation and the rate of chain deposition on the crystal surface. It is noteworthy that this theory concerns the secondary nucleation occurring on preformed lamellae. It is different from the primary nucleation defined as the initiation of a new lamella from a polymer melt. In regime I which covers low undercoolings, surface nucleation is slow and is the limiting factor while chain mobility is high. By decreasing temperature and moving to regime II, surface nucleation becomes more effective while chain movement is reduced. However the combination of the two factors gives higher growth rates. Finally, upon further cooling, we move to regime III. Contrary to regime I and due to high undercoolings, surface nucleation is maximum and chain motion is the limiting factor, resulting in lower growth rates compared to regime II. According to this theory, the crystal growth rate (G) of a homopolymer is given by:

$$G = G_0 e^{-U*/(R(T_c - T_\infty))} e^{-K_g/(T_c \Delta T f)} \quad (8)$$

where G_0 is a pre-exponent constant known as front factor, U^* is the activation energy for local motion, R is the gas constant, T_c is the crystallization temperature, T_∞ is the temperature at which flow ceases, ΔT is the undercooling ($T_m^0 - T_c$), and f is a factor to account the change in heat of fusion with temperature. K_g known as the nucleation constant is a parameter given by:

$$K_g = \frac{ab\sigma\sigma_e T_m^0}{k\Delta H_f} \quad (9)$$

where a is a constant that depends on the crystallization regime (2 for regime II crystallization and 4 for regime I and III), b is the surface nucleus thickness, σ is the lateral surface free energy, σ_e is the fold surface free energy, T_m^0 is the equilibrium melting temperature, ΔH_f is the heat of fusion for 100% crystallinity and k is the Boltzmann constant. Typical values of Hoffman–Lauritzen equation parameters reported for PLLA are summarized in Table 3.

Table 3
Hoffman–Lauritzen Eq. parameters for PLLA.

Parameter	Description	Value
U^*	Activation energy for local motion	6.27×10^3 J/mol [55]
R	Gas constant	8.314 J K^{-1} mol^{-1}
T_∞	Temperature at which flow ceases	T_g – 30 K
ΔT	Undercooling	$T_m^0 - T_c$
f	Factor to account the change in heat of fusion with temperature	$2T_c/(T_m^0 + T_c)$
T_m^0	Equilibrium melting temperature	(see Table 2)
b	Surface nucleus thickness	5.17×10^{-10} m [28]
σ	Lateral surface free energy	12.03×10^{-3} J m^{-2} [55]
σ_e	Fold surface free energy	60.89×10^{-3} J m^{-2} [55]
ΔH_f	Heat of fusion	(see Table 2)
k	Boltzmann constant	1.38×10^{-23} J K^{-1}

When the growth rate measurement is done for different crystallization temperatures, plotting $\ln(G) + U*/(R(T_c - T_\infty))$ vs. $1/(T_c \Delta T f)$ will lead to a linear plot where the slope is $-K_g$ and the intercept is $\ln(G_0)$. In addition, the regime change temperature can be obtained from the points of slope variation. Regime I–II transition for PLA was reported to occur at 163 [55] or 147 °C [41] while regime II–III transition occurs at 120 °C [32,41,80,81]. Furthermore, G is maximum at about 130 °C [32,53,55,80,82]. In some cases, however, an unusual behavior is reported for the variation of G with T_c for PLA where two local maxima are observed at temperatures around 105–115 °C and 125–135 °C instead of a bell-shaped curve [41,62,75,76,81,83–86]. The origin of this double peak behavior is not known exactly. Transition from regime II to III [41,81,87] or growth of α′ and α crystal structures [84] are assumed to be the main causes for such behavior. Interestingly, the temperatures for regime II–III transition and transition from pure α to a mixture of α′ and α crystal formation coincide (120 °C). Besides, there are arguments on whether the crystal structure or spherulite morphology remains the same [41,83,84] or varies for these two growth rate peaks [76].

In Table 4, some of the reported values for K_g and G_0 are summarized. Reported G_0 data are varying widely, however K_g values are more consistent. Additionally, ratios of K_g(III)/K_g(II) and K_g(I)/K_g(II) are close to the theoretical value of 2.

For high melting point polyesters, like PLA, Hoffman et al. [88] related the lateral surface free energy to chain flexibility through the following equation:

$$\sigma \cong \Delta H_f \left(\frac{a_0}{2}\right) \frac{1}{C_\infty} \quad (10)$$

where a_0 is the surface nucleus height and equals to 5.97 Å for PLA according to Kalb and Pennings [28]. C_∞ is the

Table 4
Reported front factor and nucleation constant for different crystallization regimes.

M_w (kg/mol)	D (%)	G_0 (μm/min) × 10^{-7}			$K_g \times 10^{-5}$ (K^2)			Ref.
		I	II	III	I	II	III	
150–690 (M_v)	–	2.13 × 10^6	1.56–3.38	–	4.87	2.29–2.44	–	[55]
50–200	–	–	–	–	–	1.21–2.08	–	[61]
127.4	0.4	–	–	–	–	2.4	–	[53]
22–701	0	–	1530–2700	–	8.11–11.27	4.64–5.01	6.33–9.7	[41]
101	–	–	–	–	–	1.85	4.38	[80]
26–1218	0.3–0.96	–	1.79–3.98	1780–53,200	–	2.27–2.55	4.73–5.51	[81]
124.8–151.3	0–1	–	1700–2080	–	4.52–6.32	2.41–3.46	4.78–7.01	[62]
101	–	–	–	–	–	1.85	4.38–5.97	[83]
136	0.96	–	510	–	–	3.03	–	[82]
206	0.8	–	–	–	–	3.22	6.02	[32]
27.18–28.08	–	–	3.98–8.86	7200–10,700	–	2.2–2.5	4.48–4.7	[85]

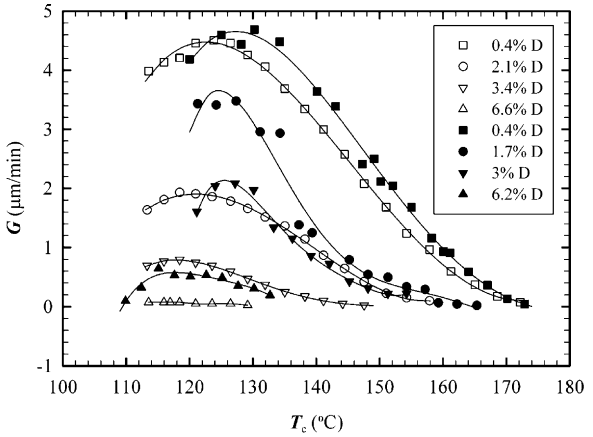

Fig. 8. Effect of D unit concentration on the spherulite growth rate of poly(LL-co-meso-lactide) (open symbols, $M_n \approx 65$ kg/mol) and poly(LL-co-DD-lactide) (filled symbols, $M_n \approx 74$ kg/mol).
Data adapted from [53,54].

characteristic ratio defined as the mean-square end-to-end distance of an unperturbed linear polymer chain over that of an equivalent random-flight chain. This ratio is a representation of chain flexibility and assumes higher values for stiffer polymer chains and more extended conformations. There is a discrepancy in the literature about PLA chain flexibility. Different values of C_∞ are reported for PLA ranging from 2 up to 12 [42,89–95]. Dorgan et al. [42,95] identified a number of reasons for this inconsistency and with a series of careful experiments in melt and solution state, they suggested that PLA has a flexible polymer chain with a characteristic ratio of about 6.5, in agreement with the simulation study by Blomqvist [94]. Presence of an oxygen atom in the backbone gives flexibility to the chain, having a nearly free-rotation around O—C bond. In terms of crystallization, this implies less extended chains that should pass a higher entropy barrier to crystallize [88]. Replacing the lateral surface free energy in Hoffman–Lauritzen model by Eq. (10) likewise confirms that for a more flexible chain (smaller C_∞), the exponential term associated to secondary nucleation becomes smaller and its contribution to growth rate is reduced.

An additional factor affecting growth rate is the D-lactate concentration. This is illustrated in Fig. 8 where the growth rate is plotted vs. crystallization temperature for PLA of similar molecular weight but with different D-lactate concentration. Open symbols represent data for which D-unit is incorporated through copolymerization of LL-lactide with meso-lactide, while filled symbols are for LL-lactide copolymerized with DD-lactide. It should be noted that the nominal concentration of meso or DD-lactide for the samples with lowest D-unit concentration were 0%. The optimum T_c (at which G is maximum) is in the 115–130 °C range. Increasing the optical impurity decreases dramatically the maximum spherulite growth rate. It is around 4.5 μm/min for a PLA with 0.4% D impurity and is decreased by a factor of 40 (less than 0.1 μm/min) with the addition of only 6.6% D-lactate. The way that D-unit is introduced into the PLA structure also influences the growth rate significantly. Comparison of the data sets with similar D-lactate concentration suggests that when DD-lactide is the source of impurity, the growth rate is higher compared to the situation where meso-lactide is the impurity source. This is logical since for DD-lactide, each two D-units are connected to each other. Thus, the average isotactic sequence length of L-units is doubled compared to the PLA having meso-lactide as the feed component (see Eq. (2)). Finally, from Fig. 8 it is clear that the optimal crystallization temperature shifts to lower values when the D-lactate concentration increases.

The molecular weight's effect on the maximum growth rate is shown in Fig. 9. The molecular weight is a number average, except for the viscosity average molecular weight data of Vasanthakumari and Pennings [55]. The data is for PLA having low D-unit concentration (0–1%). However, for some data points this parameter is not specified by the authors. Once more, we chose the general form of Flory–Fox equation for regression of the maximum growth rate data. Thereby, the following parameters were used to draw the solid-line curve in Fig. 9:

$$G_{max} = G^{\infty}_{max} - \frac{A}{M_n} \tag{11}$$

where $G^{\infty}_{max} = 1.4\ \mu m/min$ and $A = -3.8 \times 10^5\ (\mu m\ g)/(min\ mol)$.

Obviously, the growth rate decreases with molecular weight as expected from more restricted chain mobility. The decrease is sharp at lower molecular weights, while in the range of molecular weights typical of commercially

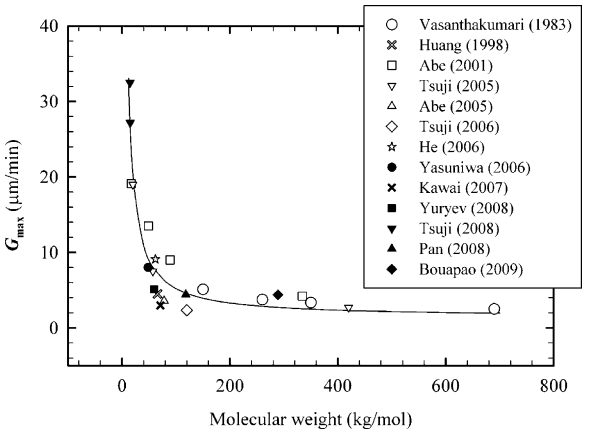

Fig. 9. Maximum spherulite growth rate as a function of molecular weight.
Data adapted from [32,41,53,55,62,72,75,76,81,82,84–86].

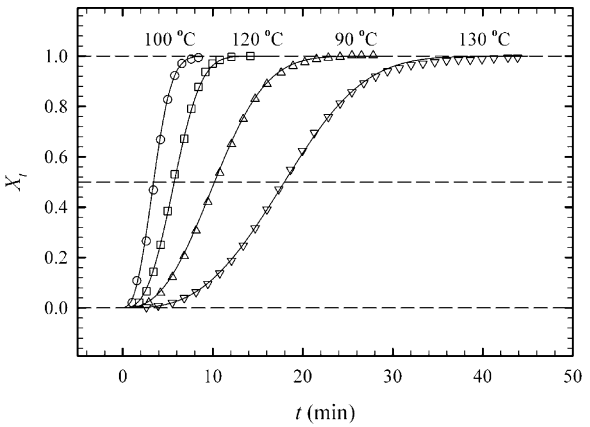

Fig. 10. Degree of crystallization of PLLA (M_n = 1.23 × 10^5 g/mol, PDI = 1.8) vs. time for different crystallization temperatures.
Data adapted from [96].

available PLA, the effect is not as dramatic as that of the optical impurity.

5.2. Kinetics through calorimetry

Calorimetry is another technique used to study the crystallization kinetics. In particular, calorimetry enables quantification of transition temperatures and enthalpies in isothermal and non-isothermal modes. For isothermal characterizations, after initial quenching below the glass transition temperature or directly from the melt state, the amorphous polymer is rapidly brought to the selected crystallization temperature T_c. Heat flow is then measured as a function of time until crystallization is completed. The heat flow data is converted into an absolute crystallinity level or more commonly, to a fraction relative to the final crystallinity level. Such crystallinity growth curves are illustrated in Fig. 10 for a PLLA crystallized at temperatures between 90 and 130 °C. Once this data is obtained, it can be curve-fitted with the Avrami model:

$$X_t = 1 - \exp[-(kt)^n] \quad (12)$$

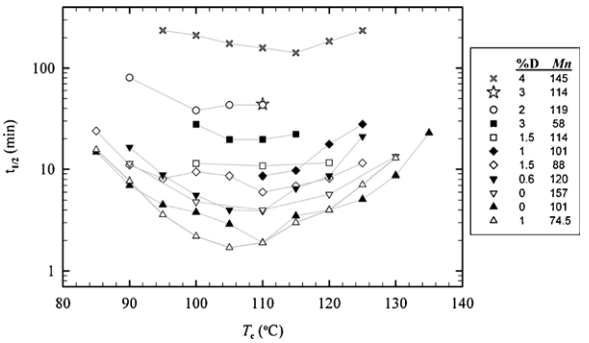

Fig. 11. Crystallization half-time as a function of crystallization temperature for different D-lactate concentrations and molecular weights.
Data adapted from [47,69,72,103,107].

where k is a kinetic rate constant and n is the Avrami exponent. The Avrami exponent is typically between 2 and 4 for polymer crystallization and is associated to the nucleation mechanism (homogeneous vs. heterogeneous and simultaneous vs. sporadic), dimensionality of crystal growth and growth mechanism, i.e., linear or diffusion controlled due to the high impurity concentration. The solid lines in Fig. 10 are data regression obtained using the Avrami model. The Avrami exponents for this specific example were in the range of 2.5–2.8 for the temperature range of 90–130 °C, suggesting a change in crystal growth from two to three dimensional with simultaneous nucleation [96]. Likewise, there are other reports of the Avrami exponent around 2 [97–99], between 2.5 and 3.5 [47,58,72,100–104] and between 3.5 and 4.3 [61,105,106]. The higher n values are attributed to three dimensional spherulitic growth with a sporadic or a combination of sporadic and simultaneous nucleation type, while the lower values are associated to two dimensional growth with instantaneous and some sporadic nucleation.

To rapidly compare the crystallization rates of materials, it is convenient to report the crystallization half-time ($t_{1/2}$) defined as the time required to attain half of the final crystallinity (X_t = 0.5). The half-time is typically reported as a function of temperature enabling the determination of the optimal temperature window. In Fig. 11, $t_{1/2}$ is plotted vs. crystallization temperature for PLA having different molecular weights (M_n in kg/mol) and D-lactate concentration. Even though the materials varied widely in terms of molecular weight and optical purity, all curves go through the typical minimum. This minimum is associated to the competition between the increased mobility and the reduced nucleation rate as a function of temperature. The lowest reported half-time was in the 2–3 min range. This is relatively high compared to other semi-crystalline commodity polymers. The half-time increases clearly with the D-lactate content and the typical U-shaped curves are shifted up. A useful general rule reported by Kolstad [47] is that the crystallization half-time increases by about 45% for each 1% increase in meso-lactide content. The data in Fig. 11 does not enable a systematic evaluation of molecular weight effects but one-to-one comparison of data with similar D-contents show that the half-time was increased

with molecular weight as expected from the reduced chain mobility.

The maximum crystallization rate, or the minimum half-time, was reached in the 105–110 °C range. It is noteworthy that the optimal crystallization temperature observed by isothermal calorimetry is 15–20 °C lower than the one determined from in situ spherulite growth rate measurement reviewed earlier. Also, the dual peaks sometimes reported for the growth rate are not observed in half-time curves. This illustrates the fact that the overall crystallization rate measured by calorimetry takes into account the increased number of crystallization sites emerging by reducing the temperature. It is also in agreement with the trend observed in Fig. 7 where spherulite density sharply decreases above 110 °C. Therefore, at temperatures lower than the optimal growth rate temperature, the crystal growth rate decrease was compensated by a larger number of crystallization sites (higher nuclei density) due to increased driving force for nucleation.

Although it has a negative effect on total crystallinity and melting point, higher crystallization rates have been observed for branched PLA compared to linear one [23,46]. The cold crystallization temperature was decreased and the crystallization peak was shifted to higher temperatures for branched PLA compared to the linear structure as a consequence of the nucleating effect of branching points. In addition, the magnitude of both the cold crystallization peak and crystallization peak upon cooling was increased due to the faster overall crystallization rate. It was also observed that increasing the branching level intensified the shifts of T_c and T_{cc} as well as peak amplitude.

6. PLA heterogeneous nucleation and plasticization

6.1. Nucleation

As discussed above, the overall nucleation and crystallization rates of PLA in homogeneous conditions are relatively low. This has prompted tremendous efforts in the scientific community toward the improvement of PLA crystallization kinetics by adding nucleants to increase its nucleation density and by adding plasticizers to increase chain mobility. Nucleating agents will reduce the nucleation induction period and increase the number of primary nucleation sites. In a general classification, nucleation can be either physical or chemical. The physical agents can be categorized as mineral, organic and mineral-organic hybrids. The different classes of nucleating agents are explained hereafter. It is noteworthy that the additional processing step required to blend additives into PLA may lead to molecular weight reduction by hydrolytic or thermal degradation. Therefore care must be taken in distinguishing between nucleation, plasticization and molecular weight reduction effects.

6.1.1. Chemical nucleating agents

Chemical nucleating agents are those for which nucleation proceeds through a chemical reaction mechanism. For example, Legras and co-workers [108–110] studied the nucleating effect of organic salts of sodium on the crystallization of polyesters such as PET and PC. They showed that when sodium 2-chlorobenzoate is added to PET, it dissolves in the polymer melt and reacts with ester linkages through a chain scission mechanism to produce sodium-terminated ionomers. Acceleration in crystallization kinetics was associated to the decrease in molecular weight and to the association of ionic end-groups into clusters, the latter being more important. Garcia [111] and Zhang [112] did similar studies on the chemical nucleation of organic sodium salts on PET and PTT respectively. In the case of PLA, sodium salts such as sodium stearate have been explored for nucleating PLA crystallization but failed to provide significant improvement of the crystallization rate while severely decreasing the PLA viscosity due to extensive chain scission [69]. Another sodium salt investigated for this purpose was sodium benzoate [113]. At a concentration of 0.2%, it reduced the M_w of PLA from 163.3 to 127.5 kg/mol, yet no enhancement in crystallization kinetics was observed.

6.1.2. Mineral nucleating agents

Talc is an effective physical nucleating agent for PLA and is commonly used as a reference to compare the nucleation ability of other additives [2,47,69,73,114–119]. For example, Kolstad [47] found that 6% talc increased the nucleation density by 500 times. This led to a 7 folds reduction in crystallization half-time, $t_{1/2}$, at the optimum crystallization temperature. In another study, a 35-fold reduction in $t_{1/2}$ with 1% talc was reported [69]. In addition, the optimum crystallization temperature was shifted from 100 to 120 °C in presence of talc [117]. In non-isothermal condition, the crystallization peak upon cooling ($T_{c.}$) is also shifted to higher temperatures. For example, it was reported that for the investigated cooling rates up to 80 °C/min, T_c was increased by 2–3 °C with increasing talc concentration from 1 to 2%. Further addition provided only an additional T_c increase of 0.5 °C/% talc indicating that relatively low talc amounts are sufficient for nucleation [69]. In another report using a low cooling rate of 1 °C/min, it was shown that the peak crystallization temperature was shifted from 107 to 123 °C when 3% talc was incorporated via solution blending [118].

Clay has been employed to improve thermal, mechanical and barrier properties of polymers. It is therefore interesting to examine its effect on the crystallization of PLA. In a qualitative study, narrowing of cold crystallization peaks were observed for PLA in presence of clay [120]. In another study, a crystallization rate increase around 50% was reported in presence of 4% organically modified montmorillonite [121]. The effect of clay exfoliation on crystallization was investigated by employing four different organo-modified clays. It was shown that the crystallinity and nucleation density of intercalated and flocculated samples were greater than those of nearly exfoliated clay. On the other hand, exfoliation of the silicate layers resulted in a lowering by about 10 °C of the cold crystallization temperature compared to intercalated morphology [122]. Krikorian and Pochan confirmed that the exfoliated morphology had a lower nucleation effect but showed that the spherulite growth rate was increased in presence of exfoliated morphology [123]. They later used FTIR spectroscopy to identify the origin of these phenomena and concluded

that in pure PLLA the inter-chain interactions precede helix formation, while for intercalated morphology inter and intra-chain interactions are simultaneous leading to faster crystallization. On the other hand, in exfoliated morphology, the helix formation started earlier and the silicate layers hindered the inter-chain interactions necessary for crystal nucleation [124]. The Avrami exponent was also used to demonstrate the effect of clay exfoliation on PLA crystallization. In the optimum crystallization temperature range, natural clay with poor dispersion increased the exponent by about one unit implying a nucleation effect while the exponent was reduced relative to the neat PLA reference for organoclays due to the restriction of crystal growth [125]. Compared to talc, clay is a less efficient nucleating agent for PLA as the reduction in $t_{1/2}$ is moderate in isothermal mode and it is not effective for high cooling rates in non-isothermal crystallization.

6.1.3. Organic nucleants

Organic materials can also physically nucleate the crystallization of PLA. This is typically achieved by adding a low molecular weight substance that will crystallize more rapidly and at a higher temperature than the polymer, providing organic nucleation sites. It was reported that calcium lactate could increase the crystallization rate of an L-lactide/meso-lactide copolymer containing 10% meso-lactide [126]. This was not corroborated however by later work from Li and Huneault where calcium lactate was compared with talc and sodium stearate [69]. Stronger nucleation effects were reported by Nam et al. using N,N-ethylenebis(12-hydroxystearamide), (EBHSA) on a PLLA with 0.8% *D* content [127]. Upon heating at 5 °C/min, the cold crystallization temperature (T_{cc}) was reduced from 100.7 to 79.7 °C, showing that EBHSA can play a nucleating role. Cold crystallization is an experiment where the sample is heated from the solid amorphous state rather than cooled from the melt state. Optical micrographs at the interface of PLA and EBHSA showed a well-developed layer of trans-crystallites grown from EBHSA surface, an evidence for epitaxial crystallization of PLA. Since EBHSA crystallizes rapidly, it acted as nucleating agent given the condition that the isothermal crystallization was carried out below the melting point of EBHSA (144.5 °C). At high crystallization temperatures (130 °C), the nucleation density in presence of EBHSA was increased 40 times and the overall crystallization rate was increased 4 times. One advantage of organic nucleating agents is that they can be very finely dispersed in molten PLA. Nakajima et al. took advantage of this point to prepare haze-free crystalline PLA [128]. Different derivatives of 1,3,5-benzene tricarboxyamide (BTA) were solution blended with PLA and screened based on the solubility parameter and melting point characteristics in a cold crystallization experiment. PLA sheets with 1% of selected derivatives crystallized at 100 °C for 5 min exhibited 44% crystallinity while the neat PLA reference showed a crystallinity of 17% in the same conditions. More interestingly, the derivative with a lower melting point (206 °C) than processing temperature (235 °C) and similar solubility parameter to PLA preserved PLA's transparency regardless of the high degree of crystallinity. Kawamoto et al. [116] compared the nucleating ability of hydrazide compounds with talc and EBHSA using a PLLA with 99.4% optical purity. Samples containing 1% nucleating agent were completely melted and their nucleation behavior was compared at a rate of 20 °C/min. Selected hydrazide compounds enabled complete PLA crystallization upon cooling with enthalpy of crystallization, ΔH_c, reaching 46 J/g. Talc and EBHSA showed ΔH_c of 26 and 35 J/g in the same conditions. The crystallization peak, T_c, was also higher for the hydrazide, 131 °C compared to 102 and 110 °C for talc and EBHSA. Finally, *p-tert*-butylcalix[8]arene is another organic material that has revealed interesting nucleating effect for PLA [104]. PLA with 1% of this material revealed a sharp crystallization peak at 134.3 °C upon cooling at a rate of 5 °C/min, 15 °C higher than that of 1% talc and nearly 26 °C higher than neat PLA. Furthermore, the Avrami exponent was increased from about 3 for neat PLA to nearly 5 for nucleated PLA as a result of change in crystal growth from spherulite to sheaf-like morphology.

6.1.4. Bio-based nucleants

Among organic nucleating agents, biobased nucleants are a particular subset of interest for PLA. Harris and Lee reported a reduction in the crystallization half-time of a 1.4% D PLA from 38 to 1.8 min when adding 2% of a vegetable-based ethylene bis-stearamide (EBS). Talc in the same conditions led to a lower half-time of 0.6 min. Upon cooling at 10 °C/min, addition of EBS enabled some crystallization with a broad and weak exotherm centered around 97 °C but again talc was more effective revealing a sharp peak at 107 °C [2].

Starch is a biopolymer that has raised a lot of interest in recent years and its blends with other polymers are under extensive investigation. The effect of starch on PLA crystallization was found to be relatively modest with a crystallization half-time reduction from 14 min to 1.8–3.2 for samples containing 1–40% starch. Again, 1% talc was found to be more efficient and decreased $t_{1/2}$ to about 0.4 min. It also shifted the optimum crystallization temperature up by around 15 °C compared to only 5 °C for starch [117].

Stronger effects were found by Li and Huneault when using starch in a thermoplastic state [129]. In this form, starch is an amorphous and highly plasticized polymer. It was found that the dispersed phase size reduction, obtained through interfacial modification, had a significant influence on PLA crystallinity. In fact, the unmodified blend comprising 20% of very coarsely dispersed thermoplastic starch did not reveal any crystallization peaks at a cooling rate of 10 °C/min. However, in the same condition, the interface modified and finely dispersed blends crystallized to their maximum level (ΔH_c = 50 J/g). In isothermal crystallization, the minimum crystallization half-time was reduced to 75 s when using an interfacial modifier.

Cellulose nanocrystal (CNC) is another emerging material that has prompted high interest due to its high tensile properties and biobased origin. It was found that unmodified CNC, with a 15 nm diameter and 200–300 nm length, did not significantly affect PLA crystallinity [103]. However, when its surface was partially silylated (SCNC), it had a modest positive effect on crystallinity. Used at 1%, the

modified CNC increased PLLA X_c from 14% to 30% upon slow cooling at 10 °C/min. In isothermal experiments, the crystallization half-time was decreased 2-fold to around 4 min when 1% SCNC was incorporated.

Orotic acid is another bio-based chemical that was recently investigated [130]. As little as 0.3% orotic acid had a significant effect on crystallinity development in non-isothermal and isothermal mode. At a cooling rate of 10 °C/min, a sharp crystallization peak at 124 °C with a high crystallization enthalpy 34 J/g was found. Besides, the $t_{1/2}$ in the 120–140 °C temperature range exhibited 10–20 fold decreases down to as low as 0.64 min. Authors believed that the good match between *b*-spacing of PLA and *a*-spacing of orotic acid crystals may explain this strong nucleating effect.

6.1.5. Carbon nanotubes (CNT)

Recently, carbon nanotubes have attracted attention because of their high aspect ratio and outstanding mechanical, thermal and electrical properties. Unmodified and modified CNT were investigated in a number of studies as nucleating agents for PLA [97,131–136]. Xu et al. [134] reported modest nucleating effects for multi-wall carbon nanotubes (MWCNT) solvent-mixed at very low loading (up to 0.08 wt.%) in PLLA. Upon cooling, the crystallization peak temperature, T_c, was shifted to higher temperatures but did not enable significant crystallinity development at cooling rates of 10 °C/min and higher. PLA-grafted carbon nanotubes (PLA-*g*-CNT) were also investigated in a PLA with 2% D [97,132]. At the moderate cooling rate of 5 °C/min, crystallinity of 12–14% were attained with 5–10% PLA-*g*-CNT [132]. Moreover, in isothermal experiments on similar material, the minimum $t_{1/2}$ was decreased from 4.2 min to 1.9 min with 5% PLA-*g*-CNT [97]. Li et al. [135] investigated the nucleating effect of maleic anhydride functionalized multi-wall carbon nanotubes on a PLA containing 4.3% *D* unit. Since the PLA had a large optical impurity, slow cooling and annealing were required to develop full crystallinity. Samples comprising the CNT exhibited sharper diffraction peaks in WAXD analysis but DSC analysis revealed that the CNT were not effective nucleating agents in moderate (i.e., 10 °C/min) or rapid cooling conditions. According to the above mentioned examples, it seems that carbon nanotubes cannot play a significant nucleating role for PLA melt processing.

6.1.6. PLA stereocomplex

As mentioned earlier, mixture of PDLA and PLLA can crystallize in the form of a stereocomplex that has a melting point about 50 °C higher than the PLLA or PDLA homocrystals. Because the stereocomplex will form at higher temperature upon cooling than the homocrystals, small concentrations of PLA stereocomplex may be suitable for nucleating PLA homo-crystallization.

Brochu et al. [137] reported that in presence of the PLA stereocomplex, the spherulite density was higher and the homopolymer crystalline fraction was larger than that in the pure polymer, implying the nucleating effect of stereocomplex crystals. They concluded that PLLA crystals can form epitaxially on stereocomplex lamellae that were previously formed at higher temperatures. Schmidt and Hillmyer [73] studied the nucleation effect of the stereocomplex for PLLA crystallization in solvent mixed blends. They used the following nucleation efficiency (NE) scale based on the self-nucleation of polymers [138] in order to quantify the nucleation performance:

$$\mathrm{NE} = \left(\frac{T_c - T_c^{\min}}{T_c^{\max} - T_c^{\min}} \right) \times 100 \tag{13}$$

$T_c^{\min}$ is the crystallization temperature observed when the neat polymer is cooled from the amorphous state. $T_c^{\max}$ is the crystallization temperature when the crystallized polymer is partially melted and self-nucleated with the remaining crystals. In this case, NE is assumed to be 100% since there is a high concentration of well distributed nucleating crystals which have a high affinity to the melt. For the investigated systems, $T_c^{\max}$ and $T_c^{\min}$ were 157 °C and 106 °C, respectively. It was shown by measuring the crystallization temperature, T_c, for various compositions that addition of small PDLA contents (forming the stereocomplex in situ in the PLLA major phase) had a higher nucleation efficiency than talc. For example, the nucleating efficiency of 6% talc was 32% whereas that of 6 wt.% PDLA was 56%. In addition, the nucleation density with as little as 0.25 wt.% PDLA was more than 170 times that of pure PLLA. The use of 1% talc only doubled the nucleation density in the same conditions. Unfortunately, the nucleation density increase was not accompanied by an overall increase in the extent of crystallization of the PLLA. This behavior was related to the tethering effect of stereocomplex crystallites, reducing PLLA chain mobility.

In another study on PLLA crystallization, Anderson and Hillmyer used the scaling concept but this time for stereocomplex formed in the melt state [115]. They quantified the effect of PDLA molecular weight (M_n equal to 5.8, 14 and 48 kg/mol) and concentration (0.5–3 wt.%) on the nucleating efficiency of the stereocomplex. The highest efficiency was observed using the 14 kg/mol PDLA. Nucleating efficiency values up to 94% were achieved when 3% of this PDLA was used, suggesting an almost ideal nucleation behavior and implying that an optimum molecular weight exists. In addition, the final crystallinity of PLLA upon cooling at 5 °C/min was increased from 41% to 60% with the addition of 0.5% of 14 kg/mol PDLA. By contrast, the addition of 6% talc led to 54% crystallinity and a nucleating efficiency of 50%. The effect of the stereocomplex on the crystallization rate of PLA at 140 °C is depicted in Fig. 12. For the lower molecular weight PLLA, the crystallization half-time, $t_{1/2}$ was reduced from 17 min to less than 1 min when 3% of a 14 kg/mol PDLA was melt blended. The same trend is observed for a higher molecular weight PLLA for which blends are prepared via solution mixing, but curves are shifted to higher half-times as a consequence of lower chain mobility. In both cases, the half-time for PDLA nucleated samples was one order of magnitude smaller than the corresponding PLA nucleated with 6% talc.

Yamane and Sasai examined the role of higher molecular weight PDLA on the nucleation and crystallization of PLLA [139]. The PLLA with M_w = 180 kg/mol was solution blended with PDLAs of 45, 120 and 260 kg/mol. Like Anderson and Hillmyer [115] and in contrast to the results

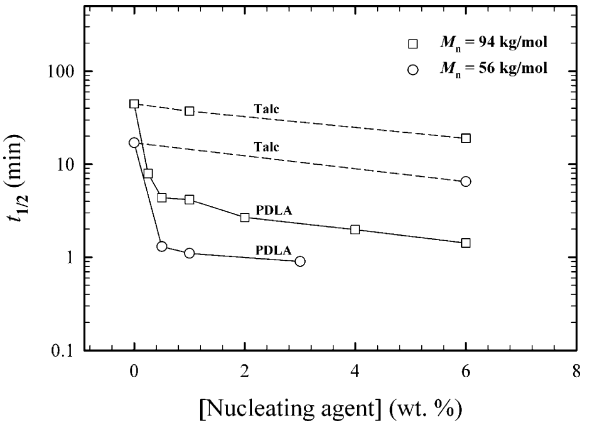

Fig. 12. $t_{1/2}$ as a function of PDLA ($M_n \approx 14$ kg/mol) and talc concentration for two PLLAs of M_n = 56 and 94 kg/mol.
Data adapted from [73,115].

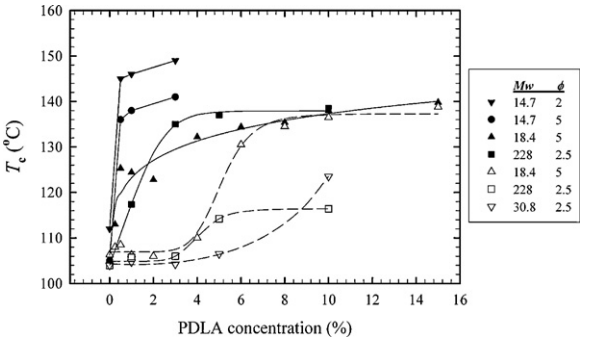

Fig. 13. Effect of PDLA concentration on peak crystallization temperature for various molecular weight and cooling rate. Solid trend lines and filled symbols: pre-crystallized stereocomplex, dashed lines and open symbols: direct stereocomplex formation from the melt.
Data adapted from [73,115,140].

obtained by Brochu et al. [137] and Schmidt and Hillmyer [73], they found that crystallinity increased with PDLA concentration when the PDLA content was very low, but tended to level off at higher PDLA concentrations. It is noteworthy that the nucleation efficiency for samples rapidly cooled from 200 °C was greater for the higher molecular weight PDLA and that this trend was reversed when the material was cooled from 240 °C. The authors explained that when cooling from temperatures below the stereocomplex melting point, the stereocomplex crystals are already present and those formed from higher molecular weight PDLA provide a larger surface area for PLLA crystallization. On the other hand, when samples are cooled from temperatures above the stereocomplex melting point, the stereocomplex has to be created within the limited timeframe of the cooling process, thus lower molecular weight PDLA is preferable because the stereocomplex is produced at a greater rate. Rahman et al. [140] also confirmed that PDLA with a lower molecular weight resulted in a higher stereocomplex crystallinity than a PDLA with higher molecular weight.

In Fig. 13, the peak crystallization temperature upon cooling as a function of PDLA concentration is compared for different cooling rates (Φ in °C/min) and PDLA molecular weights (M_W in kg/mol). Two distinct trends arise from the stereocomplex formation route. For samples in which the stereocomplex exists from the beginning of the cooling cycle, the crystallization temperature, T_c, increased with PDLA concentration up to a plateau. On the other hand, when the blends were cooled directly from the melt state without pre-existence of the stereocomplex, the nucleation effects were not observed until the PDLA concentration reached about 5%. This is due to the insufficient time to form the stereocomplex nucleation sites. Furthermore, when the cooling rate or molecular weight of PDLA was increased, T_c shifted to lower values.

Tsuji et al. [72] compared the spherulite growth rates of stereocomplex-nucleated PLA with the stereocomplex growth rate observed in their previous study [141]. They concluded that the spherulites contained only PLLA crystallites because the growth rate was independent of the PDLA content. If the spherulites had contained stereocomplex crystallites other than nucleating sites, the growth rate should have increased due to the high stereocomplex growth rate. In addition, increasing the PDLA content did not have a significant influence on the induction time. Similarly, the nucleation constant (K_g) and front constant (G_0) did not show an explicit dependence on PDLA concentration indicating no growth mechanism variation related to the presence of the stereocomplex. Tsuji et al. also compared PLA stereocomplex to other nucleants such as talc, fullerene C_{60}, clay and polysaccharides [118]. The nucleating effect was ranked in the following order: PDLA > talc > C_{60} > montmorillonite > polysaccharides.

6.1.7. Nucleation based on inorganic–organic hybrids

Inorganic–organic hybrids are a new class of materials that include polyhedral oligomeric silsesquioxane (POSS) and layered metal phosphonates. Unlike organoclays, the organic and inorganic components of these hybrid materials are connected through covalent rather than ionic bonds. In the case of POSS, the material core is constituted of a silicon and oxygen "nanocage" grafted with organic arms that can be modified depending on requirements. In a series of studies, Qiu et al. investigated the effect of POSS with isobutyl, methyl and vinyl arms on the PLA properties [142–145]. In cold crystallization experiments at a heating rate of 20 °C/min, POSS decreased the cold crystallization peak temperature, T_{cc}, between 10 and 22 °C depending on the organic arm and POSS concentration [142,144,145]. The developed crystallinity was also increased from 8 to 44%. In isothermal experiments, 1% POSS with vinyl arms decreased $t_{1/2}$ from 8 to 1.2 min [145]. Upon cooling at 5 °C/min, the crystallization temperature was increased by 10–15 °C compared to neat PLA and the samples were fully crystallized within the cooling cycle. At a cooling rate of 15 °C/min however, only a small crystallization exotherm appeared around 92 °C for 2% POSS. This was shifted slightly to 95 and 97 °C when POSS concentration was increased to 5 and 8%, respectively [144].

Layered metal phosphonates have also exhibited a nucleating effect on PLA. Pan et al. compared the nucleation effect of zinc phenylphosphonate (PPZn) to that of talc and PDLA at 1% nucleating agent content [119]. For

crystallization upon cooling at 10 °C/min, the highest crystallization temperature, around 128 °C, and the sharpest crystallization peaks were achieved for PPZn. At the same cooling rate, a very high crystallinity of 47–56% was achieved when using PPZn in the range of 0.02–15% in PLA. The cold crystallization temperature of quenched samples was also shown to be reduced by up to 30 °C when adding PPZn. In isothermal tests, PPZn was also more effective than talc and PDLA in reducing the crystallization half-time, $t_{1/2}$, of PLA. Values as low as 0.63 min were found compared to over 6 min for talc and PDLA respectively. It was suggested that the match of the lattice parameters of PPZn and PLA α crystal explains such a great enhancement of the crystallization behavior. In another study, Wang et al. investigated the effect of metal type on PLA/layered metal phosphonate composites by comparing zinc, calcium and baryum phosphonates (PPZn, PPCa and PPBa) [146]. It was found that the nucleating ability decreased in the following order PPZn > PPCa > PPBa due to the different dispersion and interfacial interaction of nucleating agents with PLA matrix.

6.2. Plasticization

Since PLA is a brittle material, plasticization has been employed extensively for toughening and extending its applications [147]. Plasticization may have contrasting effects on the crystallization behavior. On one hand, the T_g depression, a measure of plasticization efficiency, will shift the crystallization temperature window to lower temperatures. The increased chain mobility will facilitate the movement of chains from the amorphous phase unto the existing crystal surface, especially at lower temperatures. Consequently, parameters that are directly associated with chain mobility will be affected. For example in isothermal crystallization mode, spherulite growth rate should increase and the optimum growth temperature should be lowered. For cold crystallization, the crystallization peak should be sharper and shifted to lower temperatures. On the other hand, plasticization may also cause melting point and equilibrium melting point depression, adversely influencing the growth rate and overall crystallization rate at a given crystallization temperature due to the reduced degree of undercooling ($T_m^0 - T_c$) driving the crystallization and primary nucleation processes. Therefore, the enhancement in chain mobility may be partially compensated for by reduced primary and secondary nucleation.

In Table 5, average T_g and T_m depression as a function of plasticizer concentration is compared for some of the plasticizers explored for PLA.

Polyethylene glycol (PEG) is the most investigated plasticizer for PLA. It is available in a wide range of molecular weights. Copolymers of ethylene glycol or ethylene oxide with lactic acid and the possibility to have different chain termination groups are also of great interest to manipulate its properties. The addition of PEG reduces the T_g by approximately 2 °C per %plasticizer while it does not affect melting point significantly. Combination of these two characteristics makes PEG a suitable crystallization promoter for PLA. In different studies on PLA plasticization, PEG was compared to glucose monoester and partial fatty acid ester [166], to citrate ester, glycerol and oligomeric lactic acid [149] and to poly(1,3-butanediol), dibutyl sebacate and acetyl glycerol monolaurate [148]. Among these plasticizers, PEG was found to be the most efficient in decreasing the glass transition temperature and the cold crystallization temperature. Even a PLA with 5% *D* units which does not readily cold crystallize was found to cold crystallize between 88 and 90 °C with 10%PEG and up when heated at a rate of 10 °C/min [70]. The crystallinity of PLA and PEG was also found to be proportional indicating that PEG in the intra-spherulitic region crystallized much faster than that in the inter-spherulitic amorphous region. The effect of PEG end-group on plasticization and crystallization was also investigated [71,167,168]. For PEG in the lower range of M_w (400–750 g/mol) and concentrations up to 10%, the end-groups did not exhibit any significant influence on crystallization parameters such as transition temperatures, crystallinity and growth rate [71]. However, when comparing methyl–methyl, hydroxyl–hydroxyl, methyl–hydroxyl and amine–amine terminated 2000 g/mol PEG [167,168], it was found that the miscibility decreased in the following order: $2NH_2 > 2CH_3 > 1OH—1CH_3 > 2OH$. Furthermore, the melting point depression was found to increase according to the miscibility ranking. Hydroxyl-terminated PEG showed the smallest depression (3 and 7 °C for 10 and 30%) while the amine-terminated PEG showed the highest effect (14 and 26 °C for 10 and 30%). High miscibility of amine-terminated PEG with PLA and highest melting point reduction were associated to the ionic interaction of amine groups with the carboxylic acid groups at PLA chain ends. Due to the competition between chain mobility and nucleation, it was found that the crystallization half-time, $t_{1/2}$, went through a minimum when increasing the PEG content. This concentration was lower for amine-terminated PEG than other types of PEG, i.e., 10% vs. 30% plasticizer. Regarding the crystallization kinetics, contrary to the prediction based on the melting point reduction, amine-terminated PEG enabled fastest crystallization, a behavior that was attributed to the lowest fold-surface free energy when PEG has two amine end-groups compared to other end-group types.

Polypropylene glycol (PPG) is another oligomeric plasticizer investigated for PLA [150,169]. As the data in Table 5 suggests, PEG and PPG have similar effects on T_g. However, PPG may be less miscible with PLA and blends with only 12.5% PPG were shown to exhibit a second T_g around −77 °C related to a phase-separated PPG phase [150]. PPG was found to be less efficient in cold crystallization enhancement than PEG. Finally, based on the spherulite size measurements with a small angle light scattering (SALS) technique, it was shown that the growth rate and nucleation density were greater with PEG than with PPG [169].

Among the low molecular weight plasticizers for PLA, citrate esters are the most investigated ones. These materials are as effective as PEG for reducing the glass transition temperature but induce a higher melting point reduction. Among common citrates, tributyl citrate and acetyl triethyl citrate were found to be more efficient than triethyl citrate and acetyl tributyl citrate [161]. In another study, glycerin triacetate also known as triacetine was compared with the aforementioned citrate esters. It was found that tributyl citrate and triacetine led to the strongest cold

Table 5
Average T_g and T_m depression of PLA as a function of plasticizer type and concentration.

Plasticizer	Abbr.	M_w (g/mol)	ΔT_g/[Plasticizer] (°C/%)	ΔT_m/[Plasticizer] (°C/%)	Ref.
Polyethylene glycol	PEG	200	2.34	0.6	[148]
		400	2.33	0.46	[148,149]
		578	2.51		[150]
		1000	1.91	0.16	[148,151]
		1500	1.55	0.1	[149]
		8000	1.87	0	[70,152,153]
Polypropylene glycol	PPG	530	2.25		[150]
		1123	2.17		[150]
Poly(ethylene glycol-co-propylene glycol)	PEPG	12,000	1.78	0.13	[154]
Triphenyl phosphate	TPP	326.3	1.34	0.37	[155]
Dioctyl phthalate	DOP	390.56	1.75	0.46	[156]
Di-2-etylhexyladipate	DOA	371	1.48	0.4	[157–159]
Polymeric adipate	G206/2	1532	1.76	0.23	[157]
	G206/3	2000	1.96	0.4	[158,159]
	G206/5	2700	1.48		[158]
	G206/7	2565–3400	1.75	0.26	[157–159]
Poly(1,3-butylene adipate)	PBA	1500–3000	1.03		[160]
Triethyl citrate	TEC	276	1.45	0.81	[161,162]
Tributyl citrate	TBC	360	1.85	0.43	[161–164]
TBC- oligoester	TBC-3	980–4450	1.27	0.3	[163,164]
	TBC-7	2200–63,600	0.6	0.2	[163,164]
Acetyl triethyl citrate	ATEC	318	1.28	0.39	[161,162]
Acetyl tributyl citrate	ATBC	402	2	0.46	[160–162]
Glycerol			0.33	0.78	[149]
Oligomeric lactic acid	OLA	–	2.05	0.9	[149]
Poly(1,3-butanediol)	PBOH	2100	1.2	0.12	[148]
Acetyl glycerol monolaurate	AGM	358	1.54	0.36	[148]
Dibutylsebacate	DBS	314	1.53	0.45	[148]
Diethyl bishydroxymethylmalonate	DBM	220	1.67	0.57	[163,165]
DBM-oligoester	DBM-A-8	4200	0.87	0.2	[163]
	DBM-A-18	8900	0.67	0.2	[163]
	DBM-S-4	1800	1.07	0.4	[163]
	DBM-S-7	3500	0.8	0.27	[163]
	DBMAT	2300	0.87	0.2	[163]
DBM-oligoesteramide	DBMATA	3200	1.13	0.4	[163]
Glyceryl triacetate	GTA	218.2	1.85	0.59	[159,162]

crystallization temperature decrease, from 95 to around 67–70 °C by incorporation of 20–25% plasticizer. However, no significant effect on crystallization upon cooling was observed [162]. In addition to citrate esters, other low molecular weight plasticizers such as triphenyl phosphate and dioctyl phthalate were found to enhance PLA crystallization [155,156]. In the case of triphenyl phosphate, the plasticizer used at 10, 20 and 30% reduced significantly the T_g of PLA by 14, 26 and 39 °C, respectively, and increased the spherulite growth rate. The maximum growth rate for PLA was 16.8 μm/min, appearing at 132 °C. For 10, 20 and 30% triphenyl phosphate, the growth rate was increased to 30.6, 53.4 and 52.8 μm/min and the optimum temperature was reduced to 123, 110 and 102 °C, respectively [155].

Adipates are another family of PLA plasticizers. For this group of plasticizers, the T_g decreases with plasticizer concentration only up to concentration of 10% probably due to limited miscibility with PLA. Accordingly, only modest crystallization enhancements were found when using adipate plasticization [157,159].

Even though it cannot be used as a conventional plasticizer because of its high volatility, it is interesting to note that carbon dioxide is highly soluble in PLA and has shown outstanding plasticization and crystallization enhancement effects in PLA [170–175]. This is of practical importance mainly in the extrusion foaming process where CO_2 can be used as a physical blowing agent for PLA. On a weight-basis, CO_2 is much more effective in reducing T_g than the plasticizers mentioned in Table 5. For example, Reignier et al. [172] showed that the T_g was decreased by 24 °C, 46 °C and 58 °C for 5, 10 and 15 wt.% CO_2 respectively. On a pressure basis, Takada et al. [170]

found that T_g and T_m decreased linearly with increasing CO_2 pressure at a rate of 3.66 and 2.18 °C/MPa respectively. Reignier et al. showed as well that crystallization accelerates in the chain mobility controlled region in the presence of CO_2 [172]. Similar effect of CO_2 on isothermal crystallization kinetics was reported by Yu et al. [171] where $t_{1/2}$ for cold crystallization at 70 °C was reduced sharply from about 360 min for atmospheric pressure to about 10 min by increasing CO_2 pressure to 2 MPa. In actual extrusion foaming trials, Mihai et al. have shown that a very rapid PLA crystallinity development was triggered by the presence of 6–7% CO_2. Above this concentration, highly crystalline PLA foams could be formed within the few seconds of foam formation even though the neat PLA had a crystallization half-time in excess of 40 min in quiescent conditions. This rapid crystallinity formation could not be explained solely in terms of a plasticization effect and this pointed out that additional nucleation effects, possibly from supercritical carbon dioxide clusters, were necessary to explain the dramatic rise in crystallization rate [174,175].

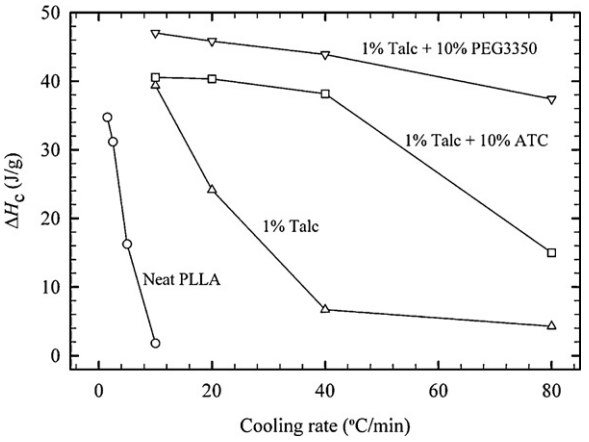

Fig. 14. Crystallization enthalpy as a function of cooling rate for different formulations.
Data adapted from [69,179].

6.3. Combination of nucleation and plasticization

The heterogeneous nucleation provided by nucleants has its greatest impact on the overall crystallization rate at elevated temperature when the driving force for homogeneous nucleation is weak. Plasticization, on the other hand, will have its highest impact at a lower temperature when crystallization is hindered by a lack of chain mobility. Therefore combination of nucleation and plasticization is expected to widen the crystallization temperature window and increase the crystallization rate of PLA. Among the first promising reports on this topic were those of Pluta [176] followed by Ozkoc et al. [177,178] focusing on blends of a 4% D PLA with combinations of up to 20% PEG and 5% clay that was either pristine or organically modified. The cold crystallization peak, T_{cc}, for samples having both modifiers appeared at approximately 80 °C which was 20 °C less than the neat PLA. Upon cooling, neat PLA and its composites with 3 or 5% clay did not reveal any crystallization peaks even at a low cooling rate of 2 °C/min. At the same rate, plasticized formulations showed some crystallization peaks, with crystallization enthalpy up to 22 J/g but this value rapidly decreased to 13 J/g when the cooling rate was increased to 15 °C/min. The peak crystallization temperature T_c was 8–9 °C lower for plasticized composites compared to plasticized PLA [178]. This is in contrast with Pluta's work showing a drop in ΔH_c and a slight increase in T_c when clay was introduced [176]. Later, Li and Huneault [69] examined combinations of talc with ATEC or PEG as plasticizers for a 2% D PLA. Much faster crystallization kinetics was achieved at 1% talc and 10% plasticizer levels than with the clay/PEG combination. Upon cooling at 10 and 20 °C/min, the materials exhibited a sharp crystallization peak around 105 °C and crystallized to their maximum level (over 40 J/g) within the cooling cycle. In comparison, sample with only 1% talc had a crystallization peak at 94 °C and reached only half of the full crystallinity. A similar study later confirmed these findings with 1% talc and up to 20% PEG [179]. Based on polarized optical micrographs obtained after non-isothermal crystallization at 2.5 °C/min from the melt, spherulite density decreased in the following order: PLA/talc > neat PLA > PLA/talc/20% PEG. Therefore, reduced nucleation due to plasticizer addition is compensated for by an increased growth rate, resulting in a higher overall crystallization rate. The effect of the plasticizer is highlighted at high cooling rates in Fig. 14. In this figure, the developed crystallinity upon cooling is depicted as a function of the cooling rate for nucleated and nucleated/plasticized samples. The crystallization enthalpy of the neat PLA control dropped sharply from 35 to nearly 0 J/g as the cooling rate was increased from 1.5 to 10 °C/min leading to essentially amorphous material. The talc filled PLA suffered a similar drop at higher cooling rates. The nucleated/plasticized formulations, however, were much less sensitive to the cooling rate. Even at a cooling rate of 80 °C/min, the formulation with talc/PEG still crystallized to a high level.

Other plasticizer/nucleant combinations lead to more moderate improvements. Instead of PEG, Xiao et al. combined talc with triphenyl phosphate plasticizer (TPP) to enhance the crystallization of a 2% D PLA [99,180]. PLA containing talc and talc + TPP showed the fastest crystallization kinetics with the development of a crystallization enthalpy around 30 J/g at a cooling rate of 10 °C/min. In isothermal conditions, the crystallization half-time, $t_{1/2}$, was reduced from 3.6 min for the neat PLA to 0.7 and 0.9 min for the nucleated and nucleated/plasticized samples, respectively. Another investigated combination was carbon nanotube (CNT) and PEG. As pointed out earlier, carbon nanotubes do not seem to provide a strong nucleating effect for PLA. Addition of up to 10% PEG to 0.5% CNT/PLA blends failed to show any significant crystallinity at cooling rates greater than 2 °C/min [181]. In addition, based on optical microscopy monitoring, it was shown that the presence of the CNT decreased the spherulite growth rate probably by restricting the PLA chain mobility.

The cooling rates investigated in differential calorimetry studies are typically far below the ones prevailing in polymer processing operations such as injection molding. In processing operations, crystallization is also preceded by

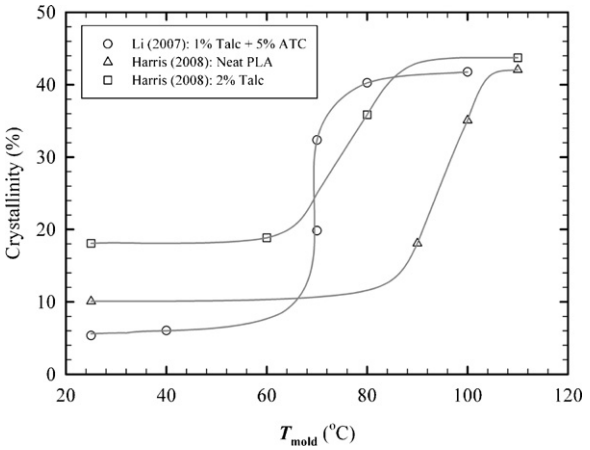

Fig. 15. Crystallinity vs. mold temperature for injection molded PLA. Data adapted from [2,69].

rapid polymer flow that can lead to strain-induced crystallization. Therefore, it is interesting to see how crystallinity can develop in typical industrial processing conditions. Fig. 15 reproduces crystallinity data as a function of the mold temperature of an injection molding process. The data from Li and Huneault [69] is for PLA with 1% talc/5% ATC molded using a 1 min cycle. The data from Harris and Lee [2] is for pure PLA and for a PLA nucleated with 2% talc but for a molding cycle of 3 min. Typically, low mold temperature will enable faster solidification of the molten material and thus will enable shorter cycle time. In the case of slow crystallizing materials, part solidification may occur through cooling below the glass transition temperature or through a significant increase in the material crystalline content. In the reported studies, quality parts were obtained at low mold temperatures, around 20–40 °C but these were essentially amorphous. At mold temperatures in the 50–60 °C range, close to PLA's T_g, the molded parts could not be ejected out of the mold because they were too soft. Finally, when maintaining the mold at 70–100 °C, highly crystallized quality parts were produced. It is noteworthy that in quiescent DSC conditions, getting fully crystallized samples in isothermal conditions below 100 °C would require a much longer time. The shearing and local orientation, inherent to the molding process, therefore had a positive effect on the final crystallinity.

The significance of shear-induced crystallinity in PLA was supported by optical microscopy observations of Li et al. on sheared PLA in isothermal [77] and non-isothermal [182] conditions. They reported that in samples pre-sheared at 1 s^{-1} and then crystallized isothermally above 120 °C, thread-like precursors first appeared and then turned into cylindrite crystals before additional spherulites started to grow. By contrast, under quiescent conditions, only spherulites were formed. Compared to the crystallization in quiescent conditions, sheared samples had lower induction time and a higher nucleation density. This morphology change was not observed however at temperatures below 120 °C probably due to the greater supercooling and thus greater homogeneous nucleation rate. In a non-isothermal test procedure, pre-sheared samples were cooled at controlled rates between 0.5 and 5 °C/min. It was found that the formation of cylindrite crystals occurred only if the shear rate used for the pre-shearing was above a certain critical value. For example, at 2 °C/min cooling, cylindrites were formed only for shear rates above 5 s^{-1}. Furthermore, the onset crystallization temperature was shifted up by as much as 30 °C by the pre-shearing. The final crystalline content was increased from 9% in quiescent conditions up to more than 30% for pre-sheared samples. Similar observations were later reported by Huang et al. [183]. Considering that the deformation rates in actual polymer processing machinery are much higher than in these model experiments, it is likely that at elevated temperature, strain-induced nucleation of PLA has a positive effect on the overall crystallization of foamed, molded or extruded PLA.

7. Conclusions

From a crystallization point of view, PLA is best viewed as a copolymer of L- and D-lactic acid with PLLA and PDLA being the limiting case homopolymers. The minor unit plays the role of a non-crystallizable co-monomer with the consequence that crystallization rate decreases dramatically with the minor unit concentration leading to amorphous materials for minor co-monomer concentration greater than 10%. The melting temperature of PLA also decreases with minor unit fraction but increases with molecular weight up to M_n values around 100 kg/mol. Conversely, its crystal growth rate is severely decreased by molecular weight in the same range. The fastest crystallization rates are observed in the 100–130 °C temperature range. A peculiar consequence of the stereoisomeric nature of lactic acid is that the PLLA and PDLA homopolymers can co-crystallize in the form of a stereocomplex that boasts a melting point that is 50 °C higher than the respective homopolymers. Numerous investigations have focused on the heterogeneous nucleation and plasticization as means to enhance the crystallization kinetics of PLA. Important nucleation rate improvements can be obtained with minerals such as talc, organics such as hydrazide compounds and organic-mineral hybrids such as layered metal phosphonates. The highest crystallization rates however were obtained when adding both nucleants and plasticizers to PLA. This widens the crystallization window and enables crystallization at high cooling rates. Further improvement in this direction will enable the development of fully crystallized extruded or injection molded applications and open the way to the production of PLA parts with greater thermal resistance.

Acknowledgement

The authors gratefully acknowledge the financial support from NSERC Network for Innovative Plastic Materials and Manufacturing Processes (NIPMMP).

References

[1] Auras R, Harte B, Selke S. An overview of polylactides as packaging materials. Macromolecular Bioscience 2004;4:835–64.

[2] Harris AM, Lee EC. Improving mechanical performance of injection molded PLA by controlling crystallinity. Journal of Applied Polymer Science 2008;107:2246–55.
[3] Perego G, Cella GD, Bastioli C. Effect of molecular weight and crystallinity on poly(lactic acid) mechanical properties. Journal of Applied Polymer Science 1996;59:37–43.
[4] Li S, McCarthy S. Influence of crystallinity and stereochemistry on the enzymatic degradation of poly(lactide)s. Macromolecules 1999;32:4454–6.
[5] Drieskens M, Peeters R, Mullens J, Franco D, Iemstra PJ, Hristova-Bogaerds DG. Structure versus properties relationship of poly(lactic acid). I. Effect of crystallinity on barrier properties. Journal of Polymer Science Part B: Polymer Physics 2009;47:2247–58.
[6] Garlotta D. A literature review of poly(lactic acid). Journal of Polymers and the Environment 2001;9:63–84.
[7] Sodergard A, Stolt M. Properties of lactic acid based polymers and their correlation with composition. Progress in Polymer Science 2002;27:1123–63.
[8] Mehta R, Kumar V, Bhunia H, Upadhyay SN. Synthesis of poly(lactic acid): a review. Polymer Reviews 2005;45:325–49.
[9] Gupta B, Revagade N, Hilborn J. Poly(lactic acid) fiber: an overview. Progress in Polymer Science 2007;32:455–82.
[10] Lim LT, Auras R, Rubino M. Processing technologies for poly(lactic acid). Progress in Polymer Science 2008;33:820–52.
[11] Chabot F, Vert M, Chapelle S, Granger P. Configurational structures of lactic acid stereocopolymers as determined by 13C-{1H} n.m.r. Polymer 1983;24:53–9.
[12] Tsuji H, Ikada Y. Stereocomplex formation between enantiomeric poly(lactic acid)s. X. Binary blends from poly(D-lactide-co-glycolide) and poly(L-lactide-co-glycolide). Journal of Applied Polymer Science 1994;53:1061–71.
[13] Wisniewski M, Borgne AL, Spassky N. Synthesis and properties of (D)- and (L)-lactide stereocopolymers using the system achiral Schiff's base/aluminium methoxide as initiator. Macromolecular Chemistry and Physics 1997;198:1227–38.
[14] Sarasua JR, Prud'homme RE, Wisniewski M, Le Borgne A, Spassky N. Crystallization and melting behavior of polylactides. Macromolecules 1998;31:3895–905.
[15] Inkinen S, Hakkarainen M, Albertsson AC, Sodergard A. From lactic acid to poly(lactic acid) (PLA): characterization and analysis of PLA and its precursors. Biomacromolecules 2011;12:523–32.
[16] Tsuji H, Ikada Y. Crystallization from the melt of poly(lactide)s with different optical purities and their blends. Macromolecular Chemistry and Physics 1996;197:3483–99.
[17] Kricheldorf HR, Serra A. Polylactones – 6. Influence of various metal salts on the optical purity of poly(L-lactide). Polymer Bulletin 1985;14:497–502.
[18] Spinu M. Star-shaped hydroxyacid polymers. US Pat 5225521, El Du Pont de Nemours Co, 1993.
[19] Kim SH, Han YK, Ahn KD, Kim YH, Chang T. Preparation of star-shaped polylactide with pentaerythritol and stannous octoate. Die Makromolekulare Chemie 1993;194:3229–36.
[20] Korhonen H, Helminen A, Seppala JV. Synthesis of polylactides in the presence of co-initiators with different numbers of hydroxyl groups. Polymer 2001;42:7541–9.
[21] Pitet LM, Hait SB, Lanyk TJ, Knauss DM. Linear and branched architectures from the polymerization of lactide with glycidol. Macromolecules 2007;40:2327–34.
[22] Wolf FK, Frey H. Inimer-promoted synthesis of branched and hyperbranched polylactide copolymers. Macromolecules 2009;42:9443–56.
[23] Mihai M, Huneault MA, Favis BD. Rheology and extrusion foaming of chain-branched poly(lactic acid). Polymer Engineering and Science 2010;50:629–42.
[24] Lehermeier HJ, Dorgan JR. Melt rheology of poly(lactic acid): consequences of blending chain architectures. Polymer Engineering and Science 2001;41:2172–84.
[25] Sodergard A, Nasman JH. Stabilization of poly(L-lactide) in the melt. Polymer Degradation and Stability 1994;46:25–30.
[26] Soedergaard A, Niemi M, Selin JF, Naesman JH. Changes in peroxide melt-modified poly(L-lactide). Industrial and Engineering Chemistry Research 1995;34:1203–7.
[27] De Santis P, Kovacs AJ. Molecular conformation of poly(S-lactic acid). Biopolymers 1968;6:299–306.
[28] Kalb B, Pennings AJ. General crystallization behaviour of poly(L-lactic acid). Polymer 1980;21:607–12.
[29] Hoogsteen W, Postema AR, Pennings AJ, Brinke Gt, Zugenmaier P. Crystal structure conformation and morphology of solution-spun poly(L-lactide) fibers. Macromolecules 1990;23:634–42.
[30] Kobayashi J, Asahi T, Ichiki M, Oikawa A, Suzuki H, Watanabe T, Fukada E, Shikinami Y. Structural and optical properties of poly lactic acids. Journal of Applied Physics 1995;77:2957–73.
[31] Zhang J, Duan Y, Sato H, Tsuji H, Noda I, Yan S, Ozaki Y. Crystal modifications and thermal behavior of poly(L-lactic acid) revealed by infrared spectroscopy. Macromolecules 2005;38:8012–21.
[32] Kawai T, Rahman N, Matsuba G, Nishida K, Kanaya T, Nakano M, Okamoto H, Kawada J, Usuki A, Honma N, Nakajima K, Matsuda M. Crystallization and melting behavior of poly(L-lactic acid). Macromolecules 2007;40:9463–9.
[33] Zhang J, Tashiro K, Tsuji H, Domb AJ. Disorder-to-order phase transition and multiple melting behavior of poly(L-lactide) investigated by simultaneous measurements of WAXD and DSC. Macromolecules 2008;41:1352–7.
[34] Cocca M, Lorenzo MLD, Malinconico M, Frezza V. Influence of crystal polymorphism on mechanical and barrier properties of poly(L-lactic acid). European Polymer Journal 2011;47:1073–80.
[35] Eling B, Gogolewski S, Pennings AJ. Biodegradable materials of poly(L-lactic acid) – 1. Melt-spun and solution-spun fibres. Polymer 1982;23:1587–93.
[36] Puiggali J, Ikada Y, Tsuji H, Cartier L, Okihara T, Lotz B. The frustrated structure of poly(L-lactide). Polymer 2000;41:8921–30.
[37] Cartier L, Okihara T, Ikada Y, Tsuji H, Puiggali J, Lotz B. Epitaxial crystallization and crystalline polymorphism of polylactides. Polymer 2000;41:8909–19.
[38] Ikada Y, Jamshidi K, Tsuji H, Hyon SH. Stereocomplex formation between enantiomeric poly(lactides). Macromolecules 1987;20:904–6.
[39] Okihara T, Tsuji M, Kawaguchi A, Katayama Ki, Tsuji H, Hyon SH, Ikada Y. Crystal structure of stereocomplex of poly(L-lactide) and poly(D-lactide). Journal of Macromolecular Science, Part B: Physics 1991;30:119–40.
[40] Cartier L, Okihara T, Lotz B. Triangular polymer single crystals: stereocomplexes twins and frustrated structures. Macromolecules 1997;30:6313–22.
[41] Abe H, Kikkawa Y, Inoue Y, Doi Y. Morphological and kinetic analyses of regime transition for poly[(S)-lactide] crystal growth. Biomacromolecules 2001;2:1007–14.
[42] Dorgan JR, Janzen J, Clayton MP, Hait SB, Knauss DM. Melt rheology of variable *L*-content poly(lactic acid). Journal of Rheology 2005;49:607–19.
[43] Jamshidi K, Hyon SH, Ikada Y. Thermal characterization of polylactides. Polymer 1988;29:2229–34.
[44] Witzke DR. Introduction to properties engineering and prospects of polylactide polymers. PhD Dissertation. E. Lansing, MI: Michigan State University, 1997.
[45] Zhao YL, Cai Q, Jiang J, Shuai XT, Bei JZ, Chen CF, Xi F. Synthesis and thermal properties of novel star-shaped poly(L-lactide)s with starburst PAMAM-OH dendrimer macroinitiator. Polymer 2002;43:5819–25.
[46] Nofar M, Zhu W, Park CB, Randall J. Crystallization kinetics of linear and long-chain-branched polylactide. Industrial and Engineering Chemistry Research 2011;50:13789–98.
[47] Kolstad JJ. Crystallization kinetics of poly(L-lactide-co-meso-lactide). Journal of Applied Polymer Science 1996;62:1079–91.
[48] Bigg DM. Polylactide copolymers: effect of copolymer ratio and end capping on their properties. Advances in Polymer Technology 2005;24:69–82.
[49] Hartmann M. High molecular weight polylactic acid polymers. In: Kaplan D, editor. Biopolymers from renewable resources. Berlin/Heidelberg: Springer-Verlag; 1998. p. 367–411.
[50] Hoffman JD, Weeks JJ. Melting process and equilibrium melting temperature of polychlorotrifluoroethylene. Journal of Research of the National Institute of Standards and Technology 1962;66A:13–28.
[51] Baur VH, Einfluß der sequenzlängenverteilung auf das schmelz-ende von copolymeren. Die Makromolekulare Chemie 1966;98:297–301.
[52] Flory PJ. Theory of crystallization in copolymers. Transactions of the Faraday Society 1955;51:848–57.
[53] Huang J, Lisowski MS, Runt J, Hall ES, Kean RT, Buehler N, Lin JS. Crystallization and microstructure of poly(L-lactide-co-meso-lactide) copolymers. Macromolecules 1998;31:2593–9.
[54] Baratian S, Hall ES, Lin JS, Xu R, Runt J. Crystallization and solid-state structure of random polylactide copolymers: poly(L-lactide-co-D-lactide)s. Macromolecules 2001;34:4857–64.
[55] Vasanthakumari R, Pennings AJ. Crystallization kinetics of poly(L-lactic acid). Polymer 1983;24:175–8.

[56] Fischer EW, Sterzel HJ, Wegner G. Investigation of the structure of solution grown crystals of lactide copolymers by means of chemical reactions. Colloid and Polymer Science 1973;251:980–90.
[57] Tsuji H, Ikada Y. Blends of isotactic and atactic poly(lactide). I. Effects of mixing ratio of isomers on crystallization of blends from melt. Journal of Applied Polymer Science 1995;58:1793–802.
[58] Iannace S, Nicolais L. Isothermal crystallization and chain mobility of poly(L-lactide). Journal of Applied Polymer Science 1997;64:911–9.
[59] Tsuji H, Ikada Y. Properties and morphologies of poly(L-lactide): 1.Annealing condition effects on properties and morphologies of poly(L-lactide). Polymer 1995;36:2709–16.
[60] Tsuji H, Ikada Y. Stereocomplex formation between enantiomeric poly(lactic acid)s. 9. Stereocomplexation from the melt. Macromolecules 1993;26:6918–26.
[61] Miyata T, Masuko T. Crystallization behaviour of poly(L-lactide). Polymer 1998;39:5515–21.
[62] Abe H, Harigaya M, Kikkawa Y, Tsuge T, Doi Y. Crystal growth and solid-state structure of poly(lactide) stereocopolymers. Biomacromolecules 2005;6:457–67.
[63] Tsuji H, Ikada Y. Stereocomplex formation between enantiomeric poly(lactic acid)s. 6. Binary blends from copolymers. Macromolecules 1992;25:5719–23.
[64] Ahmed J, Zhang JX, Song Z, Varshney SK. Thermal properties of polylactides: effect of molecular mass and nature of lactide isomer. Journal of Thermal Analysis and Calorimetry 2009;95: 957–64.
[65] Pan P, Kai W, Zhu B, Dong T, Inoue Y. Polymorphous crystallization and multiple melting behavior of poly(L-lactide): molecular weight dependence. Macromolecules 2007;40:6898–905.
[66] Yasuniwa M, Sakamo K, Ono Y, Kawahara W. Melting behavior of poly(L-lactic acid): X-ray and DSC analyses of the melting process. Polymer 2008;49:1943–51.
[67] Kim ES, Kim BC, Kim SH. Structural effect of linear and star-shaped poly(L-lactic acid) on physical properties. Journal of Polymer Science Part B: Polymer Physics 2004;42:939–46.
[68] Tsuji H, Ikada Y. Stereocomplex formation between enantiomeric poly(lactic acid)s. XI. Mechanical properties and morphology of solution-cast films. Polymer 1999;40:6699–708.
[69] Li H, Huneault MA. Effect of nucleation and plasticization on the crystallization of poly(lactic acid). Polymer 2007;48:6855–66.
[70] Hu Y, Hu YS, Topolkaraev V, Hiltner A, Baer E. Crystallization and phase separation in blends of high stereoregular poly(lactide) with poly(ethylene glycol). Polymer 2003;44:5681–9.
[71] Kulinski Z, Piorkowska E. Crystallization structure and properties of plasticized poly(L-lactide). Polymer 2005;46:10290–300.
[72] Tsuji H, Takai H, Saha SK. Isothermal and non-isothermal crystallization behavior of poly(L-lactic acid): effects of stereocomplex as nucleating agent. Polymer 2006;47:3826–37.
[73] Schmidt SC, Hillmyer MA. Polylactide stereocomplex crystallites as nucleating agents for isotactic polylactide. Journal of Polymer Science Part B: Polymer Physics 2001;39:300–13.
[74] Kikkawa Y, Abe H, Fujita M, Iwata T, Inoue Y, Doi Y. Crystal growth in poly(L-lactide) thin film revealed by in situ atomic force microscopy. Macromolecular Chemistry and Physics 2003;204:1822–31.
[75] Yuryev Y, WoodAdams P, Heuzey MC, Dubois C, Brisson J. Crystallization of polylactide films: an atomic force microscopy study of the effects of temperature and blending. Polymer 2008;49:2306–20.
[76] Yasuniwa M, Tsubakihara S, Iura K, Ono Y, Dan Y, Takahashi K. Crystallization behavior of poly(L-lactic acid). Polymer 2006;47:7554–63.
[77] Li XJ, Li ZM, Zhong GJ, Li LB. Steady-shear-induced isothermal crystallization of poly(L-lactide) (PLLA). Journal of Macromolecular Science, Part B: Physics 2008;47:511–22.
[78] Lauritzen Jr JI, Hoffman JD. Extension of theory of growth of chain-folded polymer crystals to large undercoolings. Journal of Applied Physics 1973;44:4340–52.
[79] Hoffman JD, Davis TG, Lauritzen Jr JI. The rate of crystallization of linear polymers with chain folding. In: Hannay NB, editor. Treatise on solid state chemistry: crystalline and noncrystalline solids, vol. 3. New York: Plenum Press; 1976. p. 497–614.
[80] Di Lorenzo ML. Determination of spherulite growth rates of poly(L-lactic acid) using combined isothermal and non-isothermal procedures. Polymer 2001;42:9441–6.
[81] Tsuji H, Miyase T, Tezuka Y, Saha SK. Physical properties crystallization and spherulite growth of linear and 3-arm poly(L-lactide)s. Biomacromolecules 2005;6:244–54.
[82] He Y, Fan Z, Wei J, Li S. Morphology and melt crystallization of poly(L-lactide) obtained by ring opening polymerization of L-lactide with zinc catalyst. Polymer Engineering and Science 2006;46:1583–9.
[83] Di Lorenzo ML. Crystallization behavior of poly(L-lactic acid). European Polymer Journal 2005;41:569–75.
[84] Pan P, Zhu B, Kai W, Dong T, Inoue Y. Effect of crystallization temperature on crystal modifications and crystallization kinetics of poly(L-lactide). Journal of Applied Polymer Science 2008;107:54–62.
[85] Tsuji H, Sugiura Y, Sakamoto Y, Bouapao L, Itsuno S. Crystallization behavior of linear 1-arm and 2-arm poly(L-lactide)s: effects of coinitiators. Polymer 2008;49:1385–97.
[86] Bouapao L, Tsuji H, Tashiro K, Zhang J, Hanesaka M. Crystallization spherulite growth and structure of blends of crystalline and amorphous poly(lactide)s. Polymer 2009;50:4007–17.
[87] Tsuji H, Tezuka Y, Saha SK, Suzuki M, Itsuno S. Spherulite growth of L-lactide copolymers: effects of tacticity and comonomers. Polymer 2005;46:4917–27.
[88] Hoffman JD, Miller RL, Marand H, Roitman DB. Relationship between the lateral surface free energy and the chain structure of melt-crystallized polymers. Macromolecules 1992;25:2221–9.
[89] Tonelli AE, Flory PJ. The configurational statistics of random poly(lactic acid) chains. I. Experimental results. Macromolecules 1969;2:225–7.
[90] Brant DA, Tonelli AE, Flory PJ. The configurational statistics of random poly(lactic acid) chains. II. Theory. Macromolecules 1969;2:228–35.
[91] Grijpma DW, Penning JP, Pennings AJ. Chain entanglement mechanical properties and drawability of poly(lactide). Colloid and Polymer Science 1994;272:1068–81.
[92] Joziasse CAP, Veenstra H, Grijpma DW, Pennings AJ. On the chain stiffness of poly(lactide)s. Macromolecular Chemistry and Physics 1996;197:2219–29.
[93] Cooper-White JJ, Mackay ME. Rheological properties of poly(lactides). Effect of molecular weight and temperature on the viscoelasticity of poly(L-lactic acid). Journal of Polymer Science Part B: Polymer Physics 1999;37:1803–14.
[94] Blomqvist J. RIS metropolis Monte Carlo studies of poly(L-lactic) poly(LD-lactic) and polyglycolic acids. Polymer 2001;42:3515–21.
[95] Dorgan JR, Janzen J, Knauss DM, Hait SB, Limoges BR, Hutchinson MH. Fundamental solution and single-chain properties of polylactides. Journal of Polymer Science Part B: Polymer Physics 2005;43:3100–11.
[96] Zhou WY, Duan B, Wang M, Cheung WL. Crystallization kinetics of poly(L-lactide)/carbonated hydroxyapatite nanocomposite microspheres. Journal of Applied Polymer Science 2009;113:4100–15.
[97] Shieh YT, Twu YK, Su CC, Lin RH, Liu GL. Crystallization kinetics study of poly(L-lactic acid)/carbon nanotubes nanocomposites. Journal of Polymer Science Part B: Polymer Physics 2010;48:983–9.
[98] Day M, Nawaby AV, Liao X. A DSC study of the crystallization behaviour of polylactic acid and its nanocomposites. Journal of Thermal Analysis and Calorimetry 2006;86:623–9.
[99] Xiao HW, Li P, Ren X, Jiang T, Yeh JT. Isothermal crystallization kinetics and crystal structure of poly(lactic acid): effect of triphenyl phosphate and talc. Journal of Applied Polymer Science 2010;118:3558–69.
[100] Urbanovici E, Schneider HA, Brizzolara D, Cantow HJ. Isothermal melt crystallization kinetics of poly(L-lactic acid). Journal of Thermal Analysis 1996;47:931–9.
[101] He Y, Fan Z, Hu Y, Wu T, Wei J, Li S. DSC analysis of isothermal melt-crystallization glass transition and melting behavior of poly(L-lactide) with different molecular weights. European Polymer Journal 2007;43:4431–9.
[102] Pantani R, De Santis F, Sorrentino A, De Maio F, Titomanlio G. Crystallization kinetics of virgin and processed poly(lactic acid). Polymer Degradation and Stability 2010;95:1148–59.
[103] Pei A, Zhou Q, Berglund LA. Functionalized cellulose nanocrystals as biobased nucleation agents in poly(L-lactide) (PLLA) – crystallization and mechanical property effects. Composites Science and Technology 2010;70:815–21.
[104] Wen L, Xin Z. Effect of a novel nucleating agent on isothermal crystallization of poly(L-lactic acid). Chinese Journal of Chemical Engineering 2010;18:899–904.
[105] Li Y, Chen C, Li J, Sun XS. Isothermal crystallization and melting behaviors of bionanocomposites from poly(lactic acid) and TiO_2 nanowires. Journal of Applied Polymer Science 2012;124:2968–77.

[106] Cai Y, Yan S, Yin J, Fan Y, Chen X. Crystallization behavior of biodegradable poly(L-lactic acid) filled with a powerful nucleating agent: NN-Bis(benzoyl) suberic acid dihydrazide. Journal of Applied Polymer Science 2011;121:1408–16.
[107] De Santis F, Pantani R, Titomanlio G. Nucleation and crystallization kinetics of poly(lactic acid). Thermochimica Acta 2011;522:128–34.
[108] Legras R, Mercier JP, Nield E. Polymer crystallization by chemical nucleation. Nature 1983;304:432–4.
[109] Legras R, Bailly C, Daumerie M, Dekoninck JM, Mercier JP, Zichy V, Nield E. Chemical nucleation a new concept applied to the mechanism of action of organic acid salts on the crystallization of polyethylene terephthalate and bisphenol-a polycarbonate. Polymer 1984;25:835–44.
[110] Dekoninck JM, Legras R, Mercier JP. Nucleation of poly(ethylene terephthalate) by sodium compounds: a unique mechanism. Polymer 1989;30:910–3.
[111] Garcia D. Heterogeneous nucleation of poly(ethylene terephthalate). Journal of Polymer Science Part A: Polymer Physics 1984;22:2063–72.
[112] Zhang J. Effective nucleating chemical agents for the crystallization of poly(trimethylene terephthalate). Journal of Applied Polymer Science 2004;93:590–601.
[113] Penco M, Spagnoli G, Peroni I, Rahman MA, Frediani M, Oberhauser W, Lazzeri A. Effect of nucleating agents on the molar mass distribution and its correlation with the isothermal crystallization behavior of poly(L-lactic acid). Journal of Applied Polymer Science 2011;122:3528–36.
[114] Urayama H, Kanamori T, Fukushima K, Kimura Y. Controlled crystal nucleation in the melt-crystallization of poly(L-lactide) and poly(L-lactide)/poly(D-lactide) stereocomplex. Polymer 2003;44:5635–41.
[115] Anderson KS, Hillmyer MA. Melt preparation and nucleation efficiency of polylactide stereocomplex crystallites. Polymer 2006;47:2030–5.
[116] Kawamoto N, Sakai A, Horikoshi T, Urushihara T, Tobita E. Nucleating agent for poly(L-lactic acid) – an optimization of chemical structure of hydrazide compound for advanced nucleation ability. Journal of Applied Polymer Science 2007;103:198–203.
[117] Ke T, Sun X. Melting behavior and crystallization kinetics of starch and poly(lactic acid) composites. Journal of Applied Polymer Science 2003;89:1203–10.
[118] Tsuji H, Takai H, Fukuda N, Takikawa H. Non-isothermal crystallization behavior of poly(L-lactic acid) in the presence of various additives. Macromolecular Materials and Engineering 2006;291:325–35.
[119] Pan P, Liang Z, Cao A, Inoue Y. Layered metal phosphonate reinforced poly(L-lactide) composites with a highly enhanced crystallization rate. ACS Applied Materials & Interfaces 2009;1:402–11.
[120] Ogata N, Jimenez G, Kawai H, Ogihara T. Structure and thermal/mechanical properties of poly(L-lactide)-clay blend. Journal of Polymer Science Part B: Polymer Physics 1997;35:389–96.
[121] Nam JY, Sinha Ray S, Okamoto M. Crystallization behavior and morphology of biodegradable polylactide/layered silicate nanocomposite. Macromolecules 2003;36:7126–31.
[122] Ray SS, Yamada K, Okamoto M, Fujimoto Y, Ogami A, Ueda K. New polylactide/layered silicate nanocomposites. 5. Designing of materials with desired properties. Polymer 2003;44:6633–46.
[123] Krikorian V, Pochan DJ. Unusual crystallization behavior of organoclay reinforced poly(L-lactic acid) nanocomposites. Macromolecules 2004;37:6480–91.
[124] Krikorian V, Pochan DJ. Crystallization behavior of poly(L-lactic acid) nanocomposites: nucleation and growth probed by infrared spectroscopy. Macromolecules 2005;38:6520–7.
[125] Nam PH, Ninomiya N, Fujimori A, Masuko T. Crystallization characteristics of intercalated poly(L-lactide)/organo- modified montmorillonite hybrids. Polymer Engineering and Science 2006;46:39–46.
[126] Bigg DM. Controlling the performance and rate of degradation of polylactide copolymers. In: 61st Annual Technical Conference ANTEC 2003, vol. 3. Nashville TN: Society of Plastics Engineers; 2003. p. 2816–22.
[127] Nam JY, Okamoto M, Okamoto H, Nakano M, Usuki A, Matsuda M. Morphology and crystallization kinetics in a mixture of low-molecular weight aliphatic amide and polylactide. Polymer 2006;47:1340–7.
[128] Nakajima H, Takahashi M, Kimura Y. Induced crystallization of plla in the presence of 135-benzenetricarboxylamide derivatives as nucleators: preparation of haze-free crystalline PLLA materials. Macromolecular Materials and Engineering 2010;295:460–8.
[129] Li H, Huneault MA. Crystallization of PLA/thermoplastic starch blends. International Polymer Processing 2008;23:412–8.
[130] Qiu Z, Li Z. Effect of orotic acid on the crystallization kinetics and morphology of biodegradable poly(L-lactide) as an efficient nucleating agent. Industrial and Engineering Chemistry Research 2011;50:12299–303.
[131] Moon SI, Jin F, Lee CJ, Tsutsumi S, Hyon SH. Novel carbon nanotube/poly(L-lactic acid) nanocomposites; their modulus, thermal stability, and electrical conductivity. Macromolecular Symposium 2005;224:287–95.
[132] Shieh YT, Liu GL. Effects of carbon nanotubes on crystallization and melting behavior of poly(L-lactide) via DSC and TMDSC studies. Journal of Polymer Science Part B: Polymer Physics 2007;45:1870–81.
[133] Tsuji H, Kawashima Y, Takikawa H, Tanaka S. Poly(L-lactide)/nanostructured carbon composites: conductivity, thermal properties, crystallization, and biodegradation. Polymer 2007;48:4213–25.
[134] Xu HS, Dai XJ, Lamb PR, Li ZM. Poly(L-lactide) crystallization induced by multiwall carbon nanotubes at very low loading. Journal of Polymer Science Part B: Polymer Physics 2009;47:2341–52.
[135] Li Y, Wang Y, Liu L, Han L, Xiang F, Zhou Z. Crystallization improvement of poly(L-lactide) induced by functionalized multiwalled carbon nanotubes. Journal of Polymer Science Part B: Polymer Physics 2009;47:326–39.
[136] Xu JZ, Chen T, Yang CL, Li ZM, Mao YM, Zeng BQ, Hsiao BS. Isothermal crystallization of poly(L-lactide) induced by graphene nanosheets and carbon nanotubes: a comparative study. Macromolecules 2010;43:5000–8.
[137] Brochu S, Prud'homme RE, Barakat I, Jerome R. Stereocomplexation and morphology of polylactides. Macromolecules 1995;28:5230–9.
[138] Fillon B, Lotz B, Thierry A, Wittmann JC. Self-nucleation and enhanced nucleation of polymers. Definition of a convenient calorimetric efficiency scale and evaluation of nucleating additives in isotactic polypropylene (A phase). Journal of Macromolecular Science, Part B: Physics 1993;31:1395–405.
[139] Yamane H, Sasai K. Effect of the addition of poly(D-lactic acid) on the thermal property of poly(L-lactic acid). Polymer 2003;44:2569–75.
[140] Rahman N, Kawai T, Matsuba G, Nishida K, Kanaya T, Watanabe H, Okamoto H, Kato M, Usuki A, Matsuda M, Nakajima K, Honma N. Effect of polylactide stereocomplex on the crystallization behavior of poly(L-lactic acid). Macromolecules 2009;42:4739–45.
[141] Tsuji H, Tezuka Y. Stereocomplex formation between enantiometric poly(lactic acid)s. 12. Spherulite growth of low-molecular-weight poly(lactic acid)s from the melt. Biomacromolecules 2004;5:1181–6.
[142] Qiu Z, Pan H. Preparation crystallization and hydrolytic degradation of biodegradable poly(L-lactide)/polyhedral oligomeric silsesquioxanes nanocomposite. Composites Science and Technology 2010;70:1089–94.
[143] Pan H, Qiu Z. Biodegradable poly(L-lactide)/polyhedral oligomeric silsesquioxanes nanocomposites: Enhanced crystallization mechanical properties and hydrolytic degradation. Macromolecules 2010;43:1499–506.
[144] Yu J, Qiu Z. Preparation and properties of biodegradable poly(L-lactide)/octamethyl-polyhedral oligomeric silsesquioxanes nanocomposites with enhanced crystallization rate via simple melt compounding. ACS Applied Materials & Interfaces 2011;3:890–7.
[145] Yu J, Qiu Z. Effect of low octavinyl-polyhedral oligomeric silsesquioxanes loadings on the melt crystallization and morphology of biodegradable poly(L-lactide). Thermochimica Acta 2011;519:90–5.
[146] Wang S, Han C, Bian J, Han L, Wang X, Dong L. Morphology crystallization and enzymatic hydrolysis of poly(L-lactide) nucleated using layered metal phosphonates. Polymer International 2011;60:284–95.
[147] Liu H, Zhang J. Research progress in toughening modification of poly(lactic acid). Journal of Polymer Science Part B: Polymer Physics 2011;49:1051–83.
[148] Pillin I, Montrelay N, Grohens Y. Thermo-mechanical characterization of plasticized PLA: is the miscibility the only significant factor? Polymer 2006;47:4676–82.
[149] Martin O, Averous L. Poly(lactic acid): plasticization and properties of biodegradable multiphase systems. Polymer 2001;42:6209–19.
[150] Kulinski Z, Piorkowska E, Gadzinowska K, Stasiak M. Plasticization of poly(L-lactide) with poly(propylene glycol). Biomacromolecules 2006;7:2128–35.
[151] Sungsanit K, Kao N, Bhattacharya SN. Properties of linear poly(lactic acid)/polyethylene glycol blends. Polymer Engineering and Science 2012;52:108–16.

[152] Hu Y, Rogunova M, Topolkaraev V, Hiltner A, Baer E. Aging of poly(lactide)/poly(ethylene glycol) blends. Part 1. Poly(lactide) with low stereoregularity. Polymer 2003;44:5701–10.
[153] Hu Y, Hu YS, Topolkaraev V, Hiltner A, Baer E. Aging of poly(lactide)/poly(ethylene glycol) blends. Part 2. Poly(lactide) with high stereoregularity. Polymer 2003;44:5711–20.
[154] Ran XH, Jia ZY, Yang YM, Dong LS. Flexible plasticized PLA with high crystallinity obtained by controlling the annealing temperature. e-Polymers 2010, 062/1-7.
[155] Xiao H, Lu W, Yeh JT. Effect of plasticizer on the crystallization behavior of poly(lactic acid). Journal of Applied Polymer Science 2009;113:112–21.
[156] Yang SL, Wu ZH, Meng B, Yang W. The effects of dioctyl phthalate plasticization on the morphology and thermal mechanical and rheological properties of chemical crosslinked polylactide. Journal of Polymer Science Part B: Polymer Physics 2009;47:1136–45.
[157] Martino VP, Jimenez A, Ruseckaite RA. Processing and characterization of poly(lactic acid) films plasticized with commercial adipates. Journal of Applied Polymer Science 2009;112:2010–8.
[158] Martino VP, Ruseckaite RA, Jimenez A. Thermal and mechanical characterization of plasticized poly (L-lactide-co-DL-lactide) films for food packaging. Journal of Thermal Analysis and Calorimetry 2006;86:707–12.
[159] Murariu M, Da Silva Ferreira A, Pluta M, Bonnaud L, Alexandre M, Dubois P. Polylactide (PLA)-$CaSO_4$ composites toughened with low molecular weight and polymeric ester-like plasticizers and related performances. European Polymer Journal 2008;44:3842–52.
[160] Wang N, Zhang X, Yu J, Fang J. Study of the properties of plasticised poly(lactic acid) with poly(13-butylene adipate). Polymers and Polymer Composites 2008;16:597–604.
[161] Labrecque LV, Kumar RA, Dave V, Gross RA, McCarthy SP. Citrate esters as plasticizers for poly(lactic acid). Journal of Applied Polymer Science 1997;66:1507–13.
[162] Ljungberg N, Wesslen B. The effects of plasticizers on the dynamic mechanical and thermal properties of poly(lactic acid). Journal of Applied Polymer Science 2002;86:1227–34.
[163] Ljungberg N, Wesslen B. Preparation and properties of plasticized poly(lactic acid) films. Biomacromolecules 2005;6:1789–96.
[164] Ljungberg N, Wesslen B. Tributyl citrate oligomers as plasticizers for poly (lactic acid): thermo-mechanical film properties and aging. Polymer 2003;44:7679–88.
[165] Ljungberg N, Wesslen B. Thermomechanical film properties and aging of blends of poly(lactic acid) and malonate oligomers. Journal of Applied Polymer Science 2004;94:2140–9.
[166] Jacobsen S, Fritz HG. Plasticizing polylactide – the effect of different plasticizers on the mechanical properties. Polymer Engineering and Science 1999;39:1303–10.
[167] Lai WC, Liau WB, Lin TT. The effect of end groups of PEG on the crystallization behaviors of binary crystalline polymer blends PEG/PLLA. Polymer 2004;45:3073–80.
[168] Lai WC, Liau WB, Yang LY. The effect of ionic interaction on the miscibility and crystallization behaviors of polyethylene glycol/poly(L-lactic acid) blends. Journal of Applied Polymer Science 2008;110:3616–23.
[169] Piorkowska E, Kulinski Z, Galeski A, Masirek R. Plasticization of semicrystalline poly(L-lactide) with poly(propylene glycol). Polymer 2006;47:7178–88.
[170] Takada M, Hasegawa S, Ohshima M. Crystallization kinetics of poly(L-lactide) in contact with pressurized CO_2. Polymer Engineering and Science 2004;44:186–96.
[171] Yu L, Liu H, Dean K, Chen L. Cold crystallization and post-melting crystallization of PLA plasticized by compressed carbon dioxide. Journal of Polymer Science Part B: Polymer Physics 2008;46:2630–6.
[172] Reignier J, Tatibouet J, Gendron R. Effect of dissolved carbon dioxide on the glass transition and crystallization of poly(lactic acid) as probed by ultrasonic measurements. Journal of Applied Polymer Science 2009;112:1345–55.
[173] Liao X, Nawaby AV, Whitfield PS. Carbon dioxide-induced crystallization in poly(L-lactic acid) and its effect on foam morphologies. Polymer International 2010;59:1709–18.
[174] Mihai M, Huneault MA, Favis BD, Li H. Extrusion foaming of semi-crystalline PLA and PLA/thermoplastic starch blends. Macromolecular Bioscience 2007;7:907–20.
[175] Mihai M, Huneault MA, Favis BD. Crystallinity development in cellular poly(lactic acid) in the presence of supercritical carbon dioxide. Journal of Applied Polymer Science 2009;113:2920–32.
[176] Pluta M. Morphology and properties of polylactide modified by thermal treatment filling with layered silicates and plasticization. Polymer 2004;45:8239–51.
[177] Ozkoc G, Kemaloglu S. Morphology biodegradability mechanical and thermal properties of nanocomposite films based on PLA and plasticized PLA. Journal of Applied Polymer Science 2009;114:2481–7.
[178] Gumus S, Ozkoc G, Aytac A. Plasticized and unplasticized PLA/organoclay nanocomposites: short- and long-term thermal properties morphology and nonisothermal crystallization behavior. Journal of Applied Polymer Science 2012;123:2837–48.
[179] Li M, Hu D, Wang Y, Shen C. Nonisothermal crystallization kinetics of poly(lactic acid) formulations comprising talc with poly(ethylene glycol). Polymer Engineering and Science 2010;50:2298–305.
[180] Xiao H, Yang L, Ren X, Jiang T, Yeh JT. Kinetics and crystal structure of poly(lactic acid) crystallized nonisothermally: effect of plasticizer and nucleating agent. Polymer Composites 2010;31:2057–68.
[181] Li Y, Wu H, Wang Y, Liu L, Han L, Wu J, Xiang F. Synergistic effects of PEG and MWCNTs on crystallization behavior of PLLA. Journal of Polymer Science Part B: Polymer Physics 2010;48:520–8.
[182] Li XJ, Zhong GJ, Li ZM. Non-isothermal crystallization of poly(L-lactide) (PLLA) under quiescent and steady shear conditions. Chinese Journal of Polymer Science 2010;28:357–66.
[183] Huang S, Li H, Jiang S, Chen X, An L. Crystal structure and morphology influenced by shear effect of poly(L-lactide) and its melting behavior revealed by WAXD DSC and in situ POM. Polymer 2011;52:3478–87.